nature portfolio

https://doi.org/10.1038/s41566-021-00891-y

Supplementary information

Robust, efficient, micrometre-scale phase modulators at visible wavelengths

In the format provided by the authors and unedited

Supplementary Information: Micron-Scale, Efficient, Robust Phase Modulators at Visible Wavelengths

Guozhen Liang[1,†], Heqing Huang[1,†], Aseema Mohanty[2,3], Min Chul Shin[2], Xingchen Ji[2], Michael Joseph Carter[1], Sajan Shrestha[1], Michal Lipson[2]*, and Nanfang Yu[1]*

[1]Department of Applied Physics and Applied Mathematics, Columbia University, New York, NY 10027
[2]Department of Electrical Engineering, Columbia University, New York, NY 10027
[3]Department of Electrical and Computer Engineering, Tufts University, Medford, MA 02155

*ml3745@columbia.edu *ny2214@columbia.edu
[†]These authors contributed equally to this work

I. Amplitude and phase responses of a resonator in the over-coupled regime

Assume that a micro-resonator supporting a single resonant mode is evanescently coupled to a single-mode bus waveguide (**Fig. S1a**). The complex amplitude of the resonant mode is a; the resonant frequency is ω_0; the decay rate of the resonant mode into the waveguide mode is γ_e; the decay rate of the resonant mode due to intrinsic losses in the micro-resonator is γ_o. The complex amplitudes of the waveguide mode at the input and output are s_{in} and s_{out}, respectively. No backward-propagating source is present in the waveguide, nor is the coupling between the resonant mode and the backward-propagating mode of the waveguide. According to temporal coupled-mode theory [C. Manolatou *et al*., *IEEE J. Quantum Electron.* **35**, 1322-1331 (1999)], the equations describing the evolution of the resonant mode and the output are:

$$\frac{da}{dt} = (j\omega_0 - \gamma_o - \gamma_e)a + \kappa s_{in} \quad \text{(S1)}$$

$$s_{out} = s_{in} - \kappa^* a \quad \text{(S2)}$$

where κ is the coupling coefficient of the waveguide to the resonator, which is related to γ_e by $|\kappa|^2 = 2\gamma_e$, and the constant phase difference between s_{out} and s_{in} is omitted for simplicity. Assuming that the frequency of the source is ω, we get

$$a = \frac{\kappa s_{in}}{j(\omega-\omega_0)+\gamma_o+\gamma_e} \quad \text{(S3)}$$

and

$$\frac{s_{out}}{s_{in}} = 1 - \frac{2\gamma_e}{j(\omega-\omega_0)+\gamma_o+\gamma_e}, \quad \text{(S4)}$$

from which the amplitude and phase responses of the resonant mode and the output can be extracted.

Notice that

$$\left|\frac{s_{out}}{s_{in}} - \frac{\gamma_o}{\gamma_o+\gamma_e}\right| = \frac{\gamma_e}{\gamma_o+\gamma_e}, \quad \text{(S5)}$$

which indicates that the complex transmission amplitude, $\frac{s_{out}}{s_{in}}$, is on a circle centered at $\frac{\gamma_o}{\gamma_o+\gamma_e}$ with radius $\frac{\gamma_e}{\gamma_o+\gamma_e}$ on the complex plane (**Fig. S1b**). If $\gamma_e > \gamma_o$, i.e., the resonator is in the over-coupled regime, the phase undergoes a 2π change when the resonant frequency ω_0 is tuned across the source frequency ω, i.e., $\omega - \omega_0$ sweeps from $-\infty$ to $+\infty$, as $\frac{s_{out}}{s_{in}}$ cycles along the circle from $1 - j\epsilon$ to $1 + j\epsilon$, where $\epsilon \to 0_+$ (Fig.

S1b). The complex transmission amplitude, $\frac{s_{out}}{s_{in}}$, drops to its minimum at $\omega_0 = \omega$, where the minimum amplitude can be written as $A_{min} = \frac{\gamma_e - \gamma_o}{\gamma_e + \gamma_o}$. If $\gamma_e/\gamma_o \to \infty$, i.e., the resonator is in the strongly over-coupled regime, $A_{min} \to 1$, which suggests that the variation of transmission amplitude or the device modulation loss can be reduced by increasing γ_e/γ_o. The amplitude and phase responses of a resonator in the under-coupled regime (i.e., $\gamma_e < \gamma_o$), critical-coupled regime (i.e., $\gamma_e = \gamma_o$), and strongly over-coupled regime are shown in **Figs. S1c, d** and **e**, respectively.

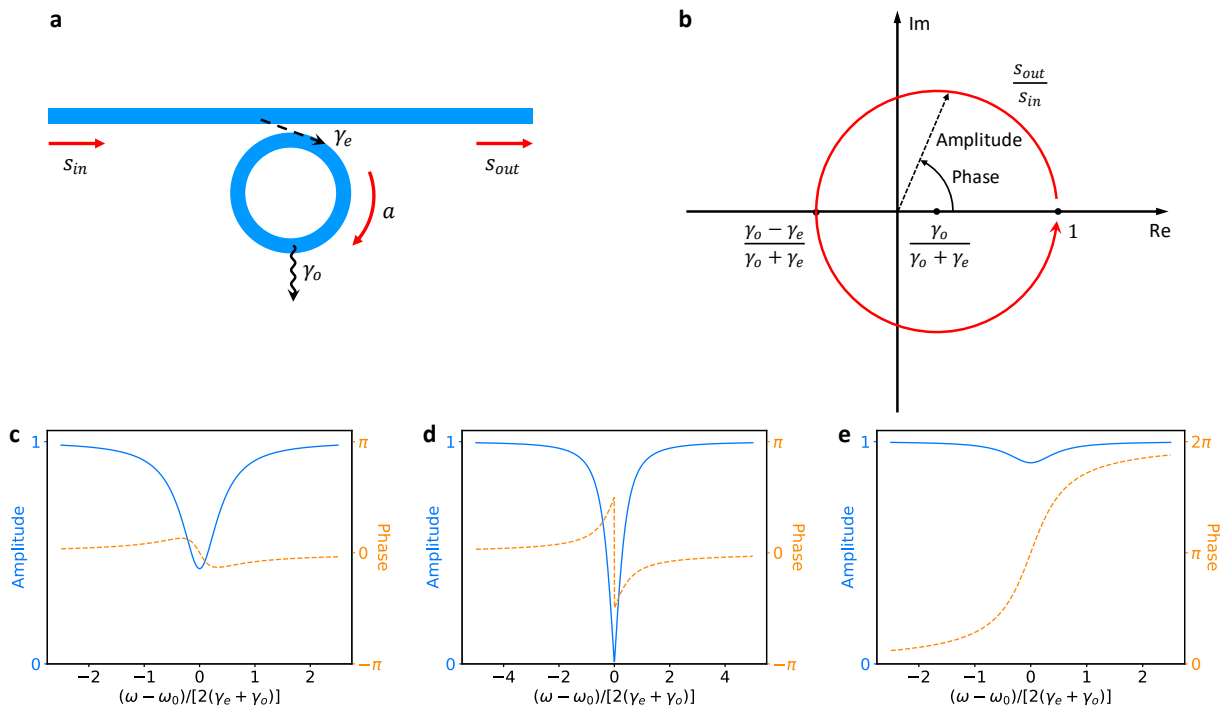

Fig. S1 | a, Schematic of the model used for temporal coupled-mode theory of a micro-resonator operating in the over-coupled regime. **b**, Complex transmission amplitude of the device in **a**. **c-e**, Calculated amplitude and phase responses of a micro-resonator operating in the under-coupled regime (**c**), critical-coupled regime (**d**), and strongly over-coupled regime (**e**). $\gamma_e/\gamma_o = 0.4$, 1, and 20 are used in (**c**), (**d**), and (**e**), respectively.

The intensity transmission at the center of the resonance, T_0, of a micro-resonator is determined by γ_e/γ_o through

$$T_0 = \left(\frac{\gamma_e/\gamma_o - 1}{\gamma_e/\gamma_o + 1}\right)^2. \text{ (S6)}$$

When a micro-resonator is in the over-coupled regime, i.e., $\gamma_e/\gamma_o > 1$, γ_e/γ_o can be calculated from measured T_0 using

$$\gamma_e/\gamma_o = \frac{1+\sqrt{T_0}}{1-\sqrt{T_0}}. \text{ (S7)}$$

The relation between T_0 and γ_e/γ_o on the linear and logarithmic scale is plotted in **Fig. S2a** and **b**, respectively. The relation between T_0 and γ_o/γ_e is plotted in **Fig. S2c**. The relation between the device modulation loss ($-10\log_{10}(T_0)$ dB) and γ_o/γ_e is plotted in **Fig. S2d**.

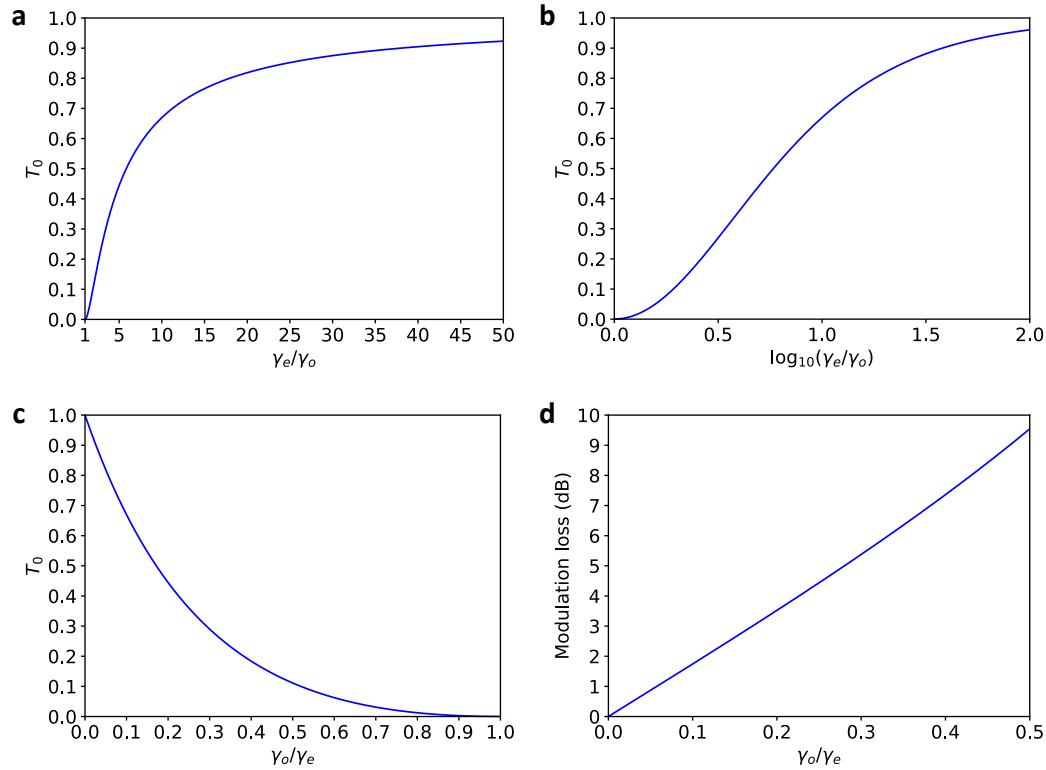

Fig. S2 | a, **b**, Relation between T_0 and γ_e/γ_o in linear scale (**a**) and log scale (**b**). **c**, Relation between T_0 and γ_o/γ_e. **d**, Relation between device modulation loss and γ_o/γ_e.

The linewidth of the resonance dip in the intensity transmission spectrum of the resonator is

$$\Delta\omega_{\text{res}} = \omega_+ - \omega_- = 2(\gamma_e + \gamma_o), \text{ (S8)}$$

where $\omega_\pm = \omega_0 \pm (\gamma_e + \gamma_o)$, because according to equation (S4), one has $\left|\frac{s_{out}}{s_{in}}\right|^2_{\omega_\pm} = \frac{(\gamma_e+\gamma_o)^2+(\gamma_e-\gamma_o)^2}{2(\gamma_e+\gamma_o)^2} = \frac{1+T_0}{2}$. The phase response at $\omega_\pm$ can then be derived using (S4) as

$$\phi_\pm = \arctan\left(\frac{\gamma_e}{\gamma_o}\right). \text{ (S9)}$$

In the strongly over-coupled regime, i.e., $\gamma_e/\gamma_o \to \infty$, $\phi_\pm \approx \pm\frac{\pi}{2}$. Thus, one can evaluate the linewidth of the resonance by monitoring the phase response curve (orange curve in **Fig. S1e**): resonance linewidth is the spectral range over which the central π phase change occurs. This could be useful in extracting linewidth from experimental data: when a resonator is deep in the strongly over-coupled regime, the dip in the intensity transmission spectrum (blue curve in **Fig. S1e**) can be hardly discernible. The linewidth is important for calculating the finesse factor of resonance, which is proportional to the reduction of thermo-

electric power consumption of thermo-optical modulators and of $V_{\pi}L$ of electro-optical modulators (Supplementary Sections IV and V).

II. Cascading two identical, uncoupled micro-resonators

The phase response of a micro-resonator in the over-coupled regime is rapid near the center of a resonance but slows down away from the center (**Fig. S3a**). As such, in thermo-optical modulators, a disproportionally larger change of heating power is needed for tuning optical phase over a larger range. This problem can be overcome by cascading two identical, uncoupled micro-resonators, which provide a total phase modulation of 4π, so that the central 2π phase shift requires a relatively small change of heating power (i.e., twice of that required for phase tuning over π in a single micro-resonator) (**Fig. S3b**).

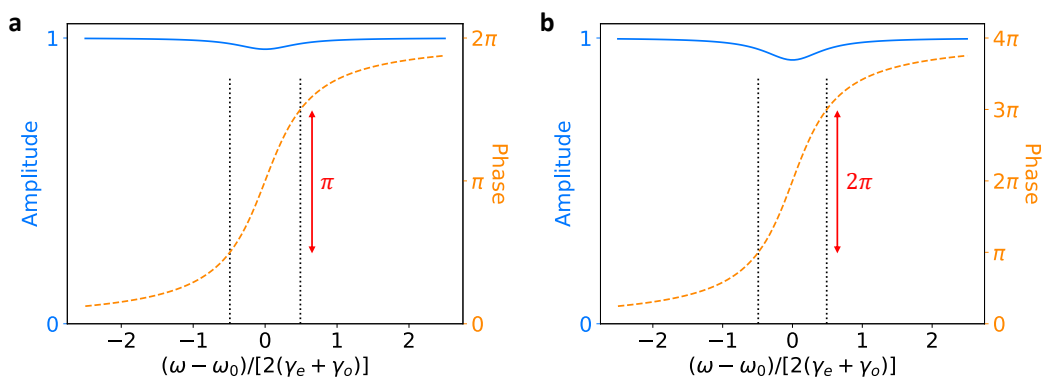

Fig. S3 | a, Calculated amplitude and phase responses of a micro-resonator operating in the over-coupled regime. The phase response is approximately linear in the central π range as a function of detuning from the center of the resonance, ω_0, and is thus approximately linear with respect to the heating power applied to a thermo-optical modulator. **b,** Calculated amplitude and phase responses of two uncoupled micro-resonators identical to the one in **a** and coupled to the same bus waveguide. The phase response is approximately linear in the central 2π range. $\gamma_e/\gamma_o = 50$ is assumed in the calculations.

III. Design considerations for adiabatic micro-ring resonators

Geometry of the adiabatic micro-ring resonators: The geometry of an adiabatic micro-ring is defined by two circles displaced from each other, and therefore characterized by an outer radius, an inner radius, and the displacement between the centers of the two circles. In a typical design, for example, the one shown in **Fig. 1d** for the blue wavelength of λ=488 nm, the outer and inner radii are 10 μm and 9 μm, respectively, and the displacement is 0.7 μm, making the narrowest section (at the coupler region) of the adiabatic ring 300 nm in width and the widest section 1.7 μm in width.

The optical mode at the wide section of the micro-ring has a reduced overlap with the sidewalls, resulting in reduced sidewall roughness scattering. The narrow section of the adiabatic micro-ring prevents the excitation of high-order resonant modes in the radial direction of the micro-ring. The transition between the narrow and wide sections is sufficiently slow (for example, the difference between the outer and inner radii never exceeds 2 μm, and the displacement never exceeds 1 μm) to ensure an adiabatic variation of the modal index; this prevents optical losses due to rapid changes of modal indices and prevents the device from entering into the chaotic operation regime with large scattering losses.

The width of the narrowest section of the adiabatic micro-ring is chosen to be close to that of the bus waveguide so that the two are phase-matched. In the design shown in **Fig. 1d**, the bus waveguide is 280 nm in width and the narrowest section of the adiabatic micro-ring is 300 nm in width. The coupling length of a directional coupler consisting of two parallel SiN waveguides both with a width of 300 nm and height of 190 nm separated by a gap of 70 nm at λ=488 nm is ~6 μm, over which a fundamental TM-waveguide mode initially injected into one waveguide is completely coupled to the other waveguide.

Coupler between bus waveguide and adiabatic micro-ring resonator: A typical gap size between a bus waveguide and a micro-ring resonator at telecommunications wavelengths is a few hundred nanometers. However, in the visible spectral range, the effective wavelength in the material can be as small as 200 nm; thus, the gap size is reduced to enhance waveguide-resonator coupling. However, excessively small gaps would cause a reduced fabrication yield and introduce a large amount of sidewall roughness during reactive ion etching. Thus, the gap size is limited to be around 100 nm (between 70 nm and 130 nm).

A conveyer belt coupler is used to improve the coupling between the bus waveguide and the resonator. In a typical design, shown in **Fig. S4a** and **b**, the coupler is composed of a $\theta_{arc} = 45°$ arc around the adiabatic micro-ring and a $L_s = 5$ μm straight segment on each side of the arc, which leads to a smooth change of the separation between the bus waveguide and the outer edge of the micro-ring changes (compared to the case when no straight waveguide segments are used) and thus helps reduce optical scattering due to abrupt modal index variations.

FDTD simulations of the transmission, coupling, and scattering loss of conveyer belt couplers with varying θ_{arc} for the adiabatic and regular micro-ring resonators are shown in **Fig. S4** and **Fig. S5**, respectively. The adiabatic micro-ring resonators have the same geometry as the one shown in **Fig. 1d**; the regular micro-ring resonators have the same outer radii as the adiabatic micro-ring resonators but have a constant width of 300 nm (**Fig. S5a** and **b**). The single-pass scattering loss of the coupler from the bus waveguide side is defined by $loss_w = 1 - t_w^2 - k_w^2$, and the single-pass scattering loss of the coupler from the micro-ring resonator side is defined by $loss_r = 1 - t_r^2 - k_r^2$, where t_w^2, k_w^2, t_r^2 and k_r^2 are defined in **Fig. S4 a-b** and **Fig. S5 a-b**.

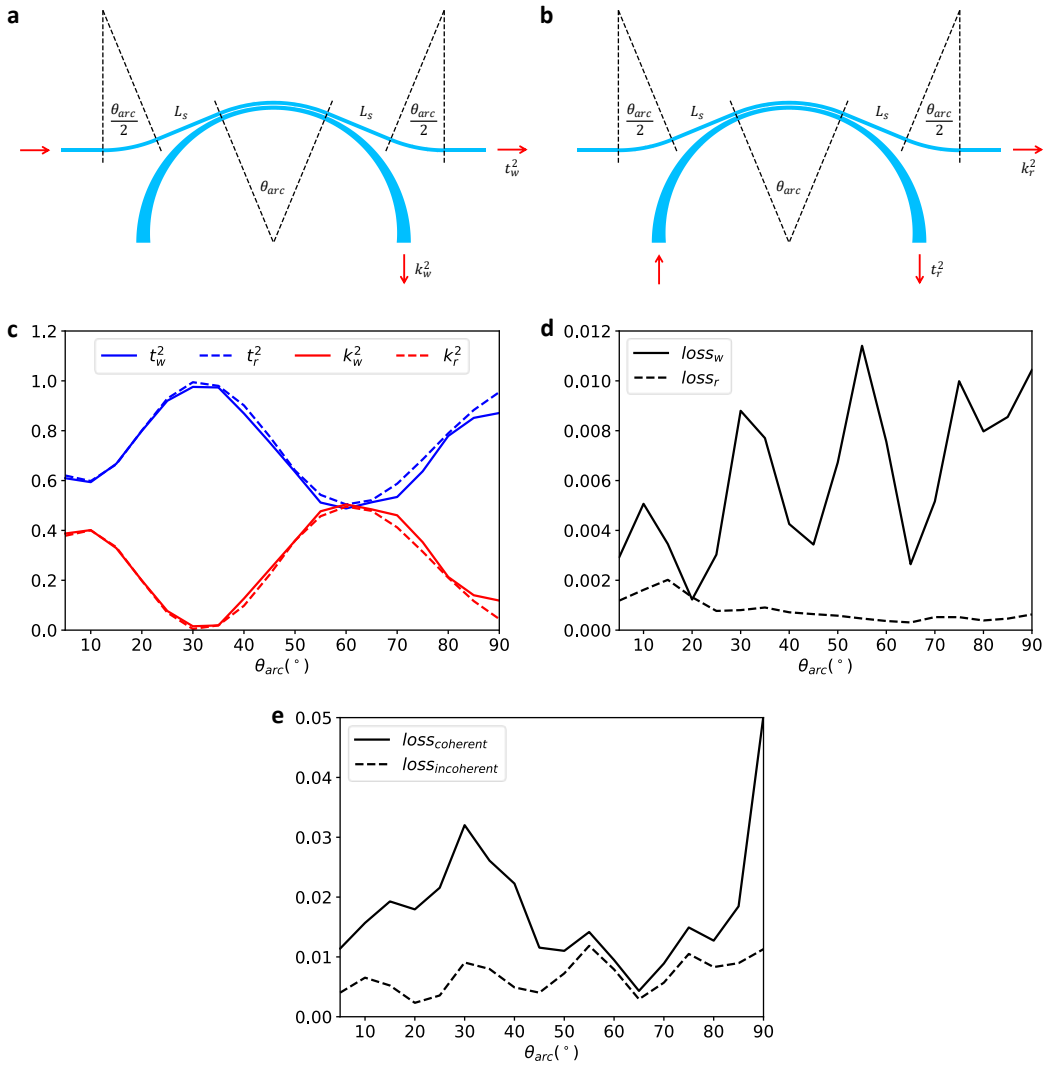

Fig. S4 | a, **b**, Schematics showing the design of a conveyer belt coupler for an adiabatic micro-ring resonator, as well as the transmission and coupling of the coupler when a TM-polarized mode is injected into the bus waveguide (**a**) and into the micro-ring (**b**). **c**, Simulated transmission and coupling of the conveyor-belt coupler with injection of light into the bus waveguide (t_w^2 and k_w^2) or into the micro-ring (t_r^2 and k_r^2) as a function of θ_{arc}. **d**, Single-pass scattering loss of the coupler with injection of light into the bus waveguide ($loss_w$) or into the micro-ring ($loss_r$). **e**, Total scattering loss of the coupler considering the circulating of the mode in the resonator, calculated using the coherent-scattering model ($loss_{coherent}$) and the incoherent-scattering model ($loss_{incoherent}$).

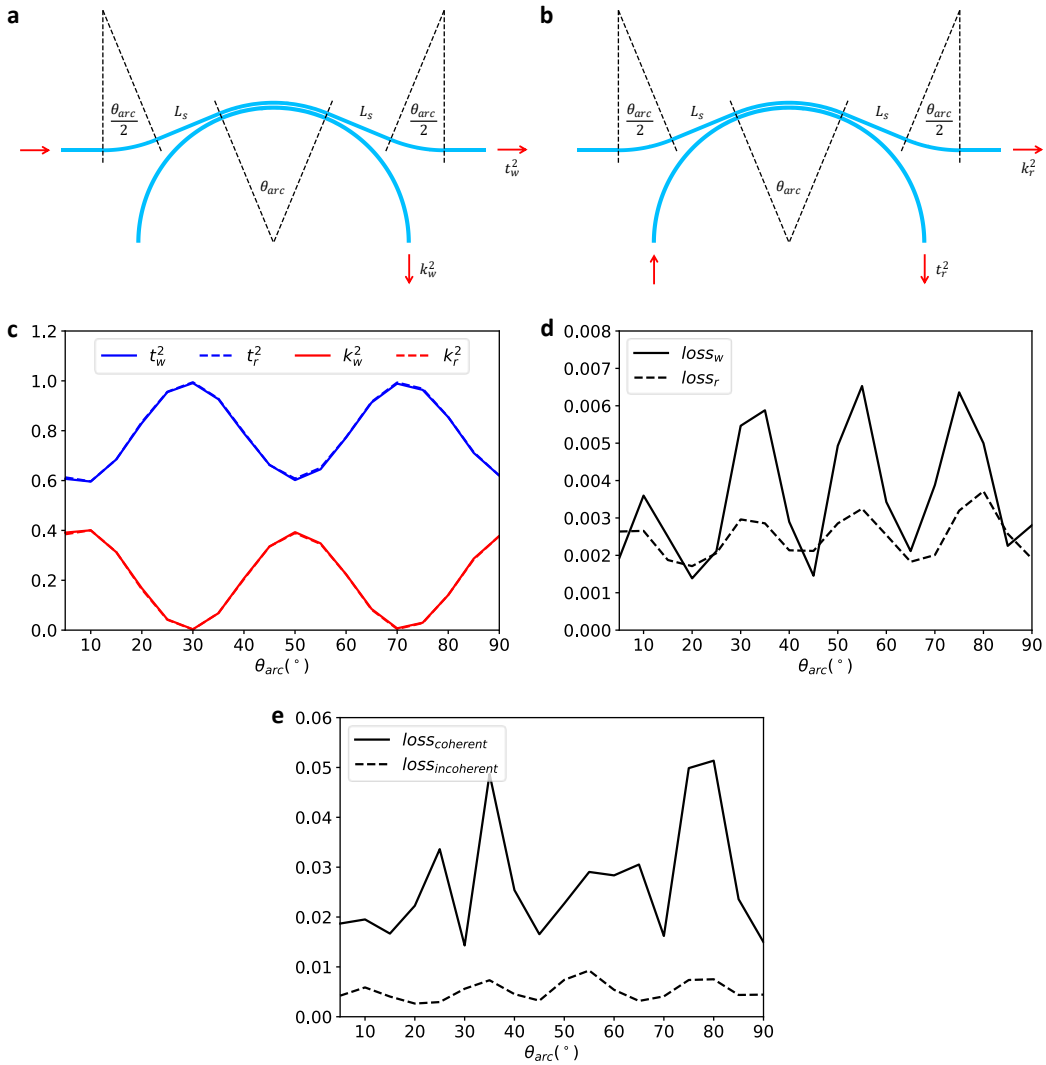

Fig. S5 | a, **b**, Schematics showing the design of a conveyer belt coupler for a regular micro-ring resonator, as well as the transmission and coupling of the coupler with injection from the waveguide side (**a**) and the micro-ring side (**b**). **c**, Simulated transmission and coupling of the conveyor-belt coupler with injection from the waveguide side (t_w^2 and k_w^2) or the micro-ring side (t_r^2 and k_r^2) as functions of θ_{arc}. **d**, Single-pass scattering loss of the coupler with injection from the waveguide side ($loss_w$) or the micro-ring side ($loss_r$). **e**, Total scattering loss of the coupler considering the circulating of the mode in the resonator, calculated using the coherent-scattering model ($loss_{coherent}$) and the incoherent-scattering model ($loss_{incoherent}$).

The total scattering loss of the coupler, considering the circulating of the mode in the resonator, is further calculated using two models: in the coherent-scattering model, the scatterings from successive circulations are assumed to accumulate coherently; in the incoherent-scattering model, the scatterings from successive circulations are assumed to accumulate incoherently. When a source in the bus waveguide with an amplitude of $s_{in}^w = 1$ enters the coupler, the amplitude of mode coupled to the micro-ring resonator is $a_0 = k_w s_{in}^w = k_w$. After a single-pass circulation in the micro-ring, the amplitude of mode re-entering the coupler

from the micro-ring side drops to $s_0^r = a \cdot a_0 = k_w a$, where a is the single-pass amplitude transmission of the circulating mode, and the amplitude of mode remaining in the micro-ring after a transmission through the coupler is $a_1 = t_r s_0^r = k_w t_r a$. Through successive circulations in the micro-ring resonator, the amplitude of the circulating mode exiting from the coupler forms a series: $\{a_n = k_w (t_r a)^n, n = 0,1,2, \dots\}$, while the amplitude of the circulating mode re-entering the coupler forms a series: $\{s_n^r = k_w a (t_r a)^n, n = 0,1,2, \dots\}$. Each time the circulating mode in the micro-ring resonator re-enters the coupler, a portion of scattering loss is generated. In the coherent-scattering model, the scattering loss of the circulating mode is summed coherently, which gives $(\sum_{n=0}^{\infty} s_n^r)^2 loss_r$, thus resulting in a total loss of $loss_{coherent} = loss_w + k_w^2 a^2/(1 - t_r a)^2 \cdot loss_r$; in the incoherent-scattering model, the scattering loss of the circulating mode is summed incoherently, which gives $\sum_{n=0}^{\infty} (s_n^r)^2\, loss_r$, thus resulting in a total loss of $loss_{incoherent} = loss_w + k_w^2 a^2/(1 - t_r^2 a^2) \cdot loss_r$.

The single-pass amplitude transmission, a, of the adiabatic and the regular micro-ring resonators are determined from the measurements on the fabricated devices shown in **Fig. 4a**, by solving the intensity transmission at the center of the resonance, $T_0 = (a - t)^2/(1 - ta)^2$, and the finesse factor, $F = \pi\sqrt{ta}/(1 - ta)$ [W. Bogaerts, *Laser Photonics Rev.* **6**, 47–73 (2012)]. For the adiabatic micro-rings, an average value of $a = 0.98$ is extracted; for the regular micro-rings, an average value of $a = 0.97$ is extracted.

For both the adiabatic and the regular devices with $\theta_{arc} = 45°$ and $L_s = 5$ μm, the coupling of the conveyer belt coupler is moderately strong (**Fig. S4c** and **Fig. S5c**), and both the single-pass scattering loss (**Fig. S4d** and **Fig. S5d**) and the total scattering loss (**Fig. S4e** and **Fig. S5e**) of the coupler are at a local minimum. The two $L_s = 5$ μm straight segments of the coupler substantially reduce the scattering losses compared to the case when the straight segments are absent (i.e., $L_s = 0$ μm) (**Fig. S6**). While the total scattering loss of the conveyer belt coupler is on the order of 1-2% (**Fig. S4e** and **Fig. S5e**), the measured total loss $1 - T_0$ (T_0 being the intensity transmission at the center of the resonance) of an adiabatic micro-ring device, including scattering due to sidewall roughness, scattering of the coupler, material absorption, and bending loss in the resonator is at best 10% and about 30% on average; this suggests that optical scattering at the coupler is not the major contributor to the total loss of the device. Since material absorption and bending losses in the resonator are negligible in our fabricated devices, the above analysis suggests that the device loss is primarily contributed by scattering at sidewall roughness. The comparative advantage of the adiabatic micro-ring is that the sidewall scattering loss is reduced to approximately 1/3 of that of the regular micro-ring (**Fig. 4a**).

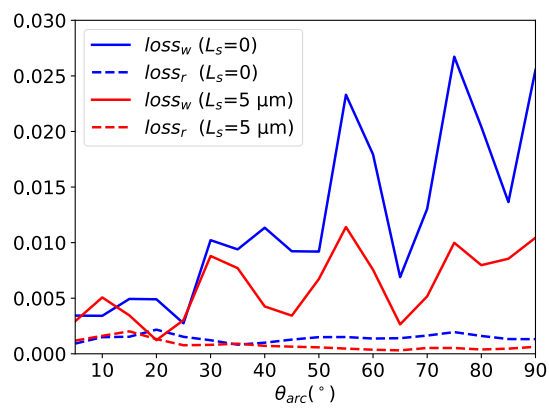

Fig. S6 | Comparison of scattering losses of a conveyer belt coupler with L_s = 5 μm and a conveyer belt coupler with L_s = 0 for adiabatic micro-ring resonators with injection from the waveguide side ($loss_w$) or the micro-ring side ($loss_r$).

IV. Comparison of thermoelectric power consumption between a micro-resonator and a straight waveguide phase shifter

The heating power needed for π phase tuning in a waveguide-based phase shifter is

$$P_{\mathrm{wg}} = p_0 \delta T_{\mathrm{wg}} L_{\mathrm{wg}}, \text{ (S10)}$$

where p_0 is the heating power to cause one degree of temperature change over one unit length of the waveguide, δT_{wg} is the temperature increase needed for π phase tuning, and L_{wg} is the waveguide length. The phase change of the waveguide-based phase shifter is

$$\delta\varphi = \frac{2\pi}{\lambda} \delta n_{\mathrm{wg}} L_{\mathrm{wg}} = \pi, \text{ (S11)}$$

where λ is the free-space wavelength and δn_{wg} is the change of the effective waveguide modal index, n_{wg}. δn_{wg} is related to δT_{wg} by the thermo-optic coefficient α_{TO}:

$$\delta n_{\mathrm{wg}} = \alpha_{\mathrm{TO}} n_{\mathrm{wg}} \delta T_{\mathrm{wg}}. \text{ (S12)}$$

The heating power for π phase tuning in a waveguide-based phase shifter can then be determined by using equations (S10)-(S12):

$$P_{\mathrm{wg}} = \frac{p_0 \lambda}{2\alpha_{\mathrm{TO}} n_{\mathrm{wg}}}. \text{ (S13)}$$

The heating power needed for π phase tuning in a phase modulator based on a strongly over-coupled resonator is

$$P_{\mathrm{ring}} = p_0 \delta T_{\mathrm{ring}} L_{\mathrm{ring}}, \text{ (S14)}$$

where δT_{ring} is the temperature increase needed for π phase tuning, and L_{ring} is the circumference of the micro-ring resonator. The phase tuning is approximately π over the linewidth of the resonance (Supplementary Section I), so that we have:

$$\frac{\delta n_{\mathrm{ring}}}{n_{\mathrm{ring}}} = \frac{\delta\lambda_{\mathrm{ring}}}{\lambda_{\mathrm{ring}}}, \text{ (S15)}$$

where $\delta\lambda_{\mathrm{ring}}$ is the linewidth of resonance in wavelength, λ_{ring} is the resonant wavelength, δn_{ring} is the change of effective modal index, n_{ring}, for π phase tuning, related to δT_{ring} by the thermo-optic coefficient α_{TO}:

$$\delta n_{\mathrm{ring}} = \alpha_{\mathrm{TO}} n_{\mathrm{ring}} \delta T_{\mathrm{ring}}. \text{ (S16)}$$

We further relate $\delta\lambda_{\mathrm{ring}}$ to the finesse factor, F, of the resonator:

$$F = \frac{\mathrm{FSR}}{\delta\lambda_{\mathrm{ring}}}, \text{ (S17)}$$

where FSR is the free spectral range of the resonator, which can be calculated by

$$\mathrm{FSR} = \frac{\lambda_{\mathrm{ring}}^2}{n_{\mathrm{ring}} L_{\mathrm{ring}}}. \text{ (S18)}$$

The heating power needed for π phase tuning in the resonator-based phase modulator can then be determined by using equations (S14)-(S18):

$$P_{\text{ring}} = \frac{p_0 \lambda_{\text{ring}}}{\alpha_{\text{TO}} n_{\text{ring}} F}. \text{ (S19)}$$

The waveguide and the micro-ring resonator have similar effective modal indices ($n_{\text{wg}} \approx n_{\text{ring}}$) and p_0; therefore, we obtain the ratio of heating power needed for π phase tuning between the waveguide-based phase shifter and the resonator-based phase modulator:

$$\frac{P_{\text{wg}}}{P_{\text{ring}}} = \frac{F}{2}. \text{ (S20)}$$

V. Comparison of $V_\pi L$ between a micro-resonator and a waveguide-based phase shifter

The change of the effective waveguide modal index for π phase tuning of an electro-optically tuned waveguide-based phase shifter is

$$\delta n_{\text{wg}} = \eta V_{\pi_\text{wg}}, \text{ (S21)}$$

where V_π is the voltage for π phase tuning, and η is the effective waveguide modal index change caused by the change of voltage by 1 volt. The half-wave voltage-length product $V_\pi L$ of the waveguide-based phase shifter can then be determined by using equations (S11) and (S21):

$$V_{\pi_\text{wg}} L_{\text{wg}} = \frac{\lambda}{2\eta}. \text{ (S22)}$$

The change of effective model index for π phase tuning of an electro-optically tuned phase modulator based on a strongly over-coupled resonator is

$$\delta n_{\text{res}} = \eta V_{\pi_\text{ring}}. \text{ (S23)}$$

$V_\pi L$ of the resonator-based phase modulator can then be determined by using equations (S15), (S17), (S18) and (S23):

$$V_{\pi_\text{ring}} L_{\text{ring}} = \frac{\lambda_0}{F\eta}, \text{ (S24)}$$

where F is the finesse factor of the resonator, and λ_0 is the resonant wavelength.

The waveguide and the micro-ring resonator have similar η; therefore, we obtain the ratio of $V_\pi L$ between the waveguide-based phase shifter and the resonator-based phase modulator:

$$\frac{V_{\pi_\text{wg}} L_{\text{wg}}}{V_{\pi_\text{ring}} L_{\text{ring}}} = \frac{F}{2}. \text{ (S25)}$$

VI. Output ports of a micro-resonator incorporated into a Mach-Zehnder interferometer

A micro-resonator is incorporated into a Mach-Zehnder interferometer (MZI) that is furnished with three output ports to monitor the amplitude and phase responses of the resonator (**Fig. S7a**). The output from the intensity port follows the transmission of the device; the output from the phase port is an interference between the device transmission and the reference waveguide; the output from the reference port is the transmission of the reference waveguide. If the micro-resonator operates in the under-coupled regime, i.e., $\gamma_e/\gamma_o < 1$, the dips in the outputs from both the phase port and the intensity port will not reach zero at the

center of resonance (**Fig. S7b**). If the micro-resonator operates in the critical-coupled regime, i.e., $\gamma_e/\gamma_o = 1$, the dip in the output from the intensity port will reach zero at the center of resonance (**Fig. S7c**). If the micro-resonator operates in the over-coupled regime, i.e., $\gamma_e/\gamma_o > 1$, the dip in the output from the phase port will reach a value close to zero, while the dip in the output from the intensity port will reach a minimum of $\left(\frac{\gamma_e/\gamma_o - 1}{\gamma_e/\gamma_o + 1}\right)^2$ (**Fig. S7d**).

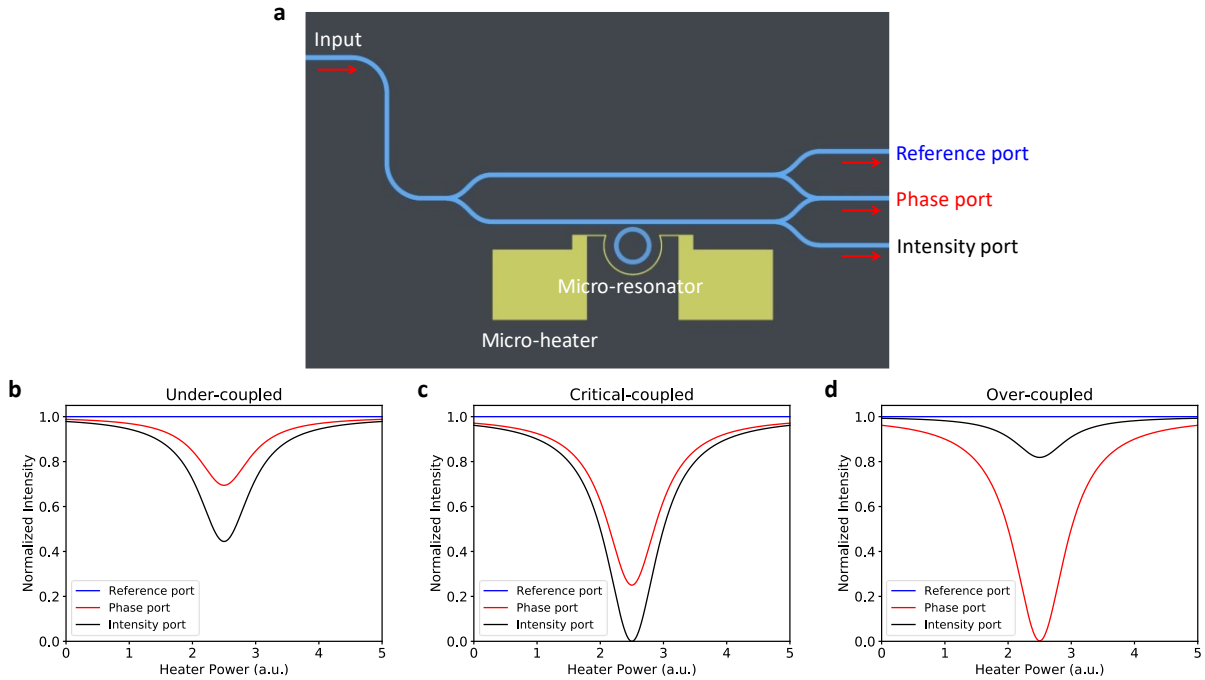

Fig. S7 | a, Schematic showing the device layout that allows for monitoring the phase and amplitude responses of a micro-resonator. **b-d,** Theoretical calculations of the outputs from the three ports of the device when the resonator operates in three distinct regimes. (**b**) $\gamma_e/\gamma_o = 0.2$, (**c**) $\gamma_e/\gamma_o = 1$, and (**d**) $\gamma_e/\gamma_o = 20$ are assumed in the calculations.

VII. Device testing

A schematic of the experimental setup used to test integrated photonic devices at the green wavelength is shown in **Fig. S8a**. The green light is produced by frequency doubling of the output of a tunable diode laser (Newport, model TLB-6721-P, tunable wavelengths of 1030-1070 nm). The output of the diode laser is amplified by a fiber amplifier (3SP Group, TKS 1064 nm CW SLM PM Fiber Amplifier) and frequency doubling is realized by using temperature-controlled periodically poled lithium niobate (PPLN). The resulting green light is coupled into the input waveguide of a device being tested using free-space optics, and the coupling loss is estimated to be 10 dB. The incident polarization is controlled by a linear polarizer. The insertion loss, that is, the static part of the optical loss that is independent from the modulation loss and due to light propagation in waveguides (~2 mm in length in total) leading into and out of the adiabatic micro-ring, is ~0.9 dB in the green spectral range.

A schematic of the experimental setup used to test integrated photonic devices at the blue wavelength is shown in **Fig. S8b**. The blue light with a wavelength of 488 nm is produced by a diode laser (Toptica, DL pro), and is coupled into the input waveguide of a device being tested using a single-mode optical fiber,

where paddles are used to control the incident polarization. The fiber-to-chip coupling loss and the insertion loss is estimated to be 10 dB and 1.9 dB, respectively.

In both setups, an aperture is used to select the signal from one of the three output ports of each device (i.e., intensity, phase, and reference ports). A Si avalanche photodetector (Thorlabs, APD120A2) is used to measure the output signal intensity.

A micro-ring device supports a plethora of resonances across the visible spectrum, some of which are blue-detuned and some are red-detuned with respect to the laser frequency. The first blue-detuned resonance with a resonant frequency closest to the laser frequency will be the chosen device resonance. Heating up the micro-ring device with its micro-heater leads to increased refractive indices of SiN, and thus a red-shift of several closest blue-detuned resonances across the laser frequency. A range of heating power continuously varying from 0 to 50 mW is usually used, and this typically sweeps two initially blue-detuned resonances across the laser frequency. The signal in the 'phase port' of the device will thus show two dips as a function of the heating power. The heating power at the first dip is the heating bias to align our target device resonance with the laser frequency; if this heating power is considered too large (i.e., > 5 mW), we will blue-shift the laser frequency to bring it closer to the first blue-detuned resonance. In this way we can reduce the heating bias needed to align the target device resonance with the laser frequency.

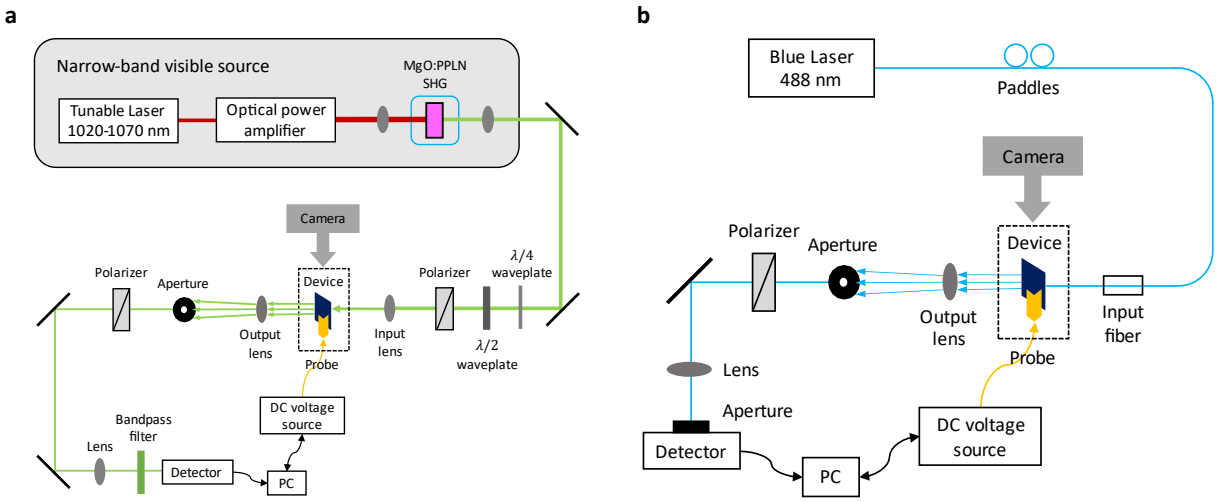

Fig. S8 | a, Schematic of the experimental setup for device testing at the green wavelength. **b,** Schematic of the experimental setup for device testing at the blue wavelength.

VIII. Micro-disc resonator at the green wavelength for phase modulation

Phase modulation is also demonstrated in micro-disc resonators operating at the green wavelength. The micro-disc resonator (**Fig. S9a**) supports quasi-TE whispering-gallery modes (**Fig. S9b**) with smaller optical scattering losses than the quasi-TE resonant modes supported by a micro-ring resonator of the same dimension. A micro-disc has only one sidewall and the whispering-gallery modes are shifted towards the disc center (**Fig. S12**); both facts lead to a weakened optical interaction with device side walls. However, reduced evanescent fields outside a micro-disc lead to a reduction of γ_e. The latter can be improved by increasing the interaction length via a conveyor belt coupler (**Figs. S9a** and **c**).

The fundamental whispering-gallery mode of a micro-disc resonator, by our design, will operate in the strongly over-coupled regime. **Figures S9d** and **e** are experimental results, showing that under such conditions a π phase shift is achieved when the heating power changes by only 0.68 mW, and that the intensity variation is limited to 1.13 dB across the resonance. The estimated intrinsic and loaded Q-factors are 3.6×10^5 and 2.2×10^4, respectively. The main drawback of the micro-disc resonator is that it commonly supports higher-order whispering gallery modes, which may not operate in the strongly over-coupled regime (**Fig. S9f**).

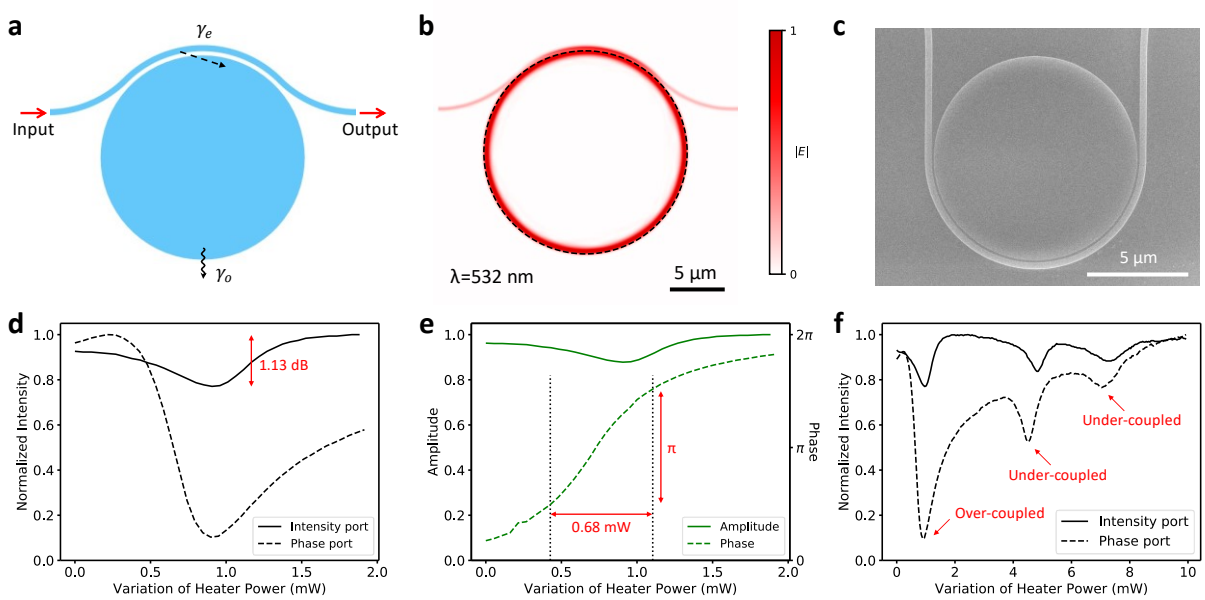

Fig. S9 | a, Design of a micro-disc resonator operating in the strongly over-coupled regime at the green wavelength. **b**, Simulated quasi-TE resonant mode of the micro-disc with the dashed curve indicating the micro-disc outline. **c**, Scanning electron micrograph of a micro-disc device. **d, e,** Measured signals from the "intensity" and "phase" ports (**d**) and extracted amplitude and phase responses (**e**) of a micro-disc resonator with a 15-μm radius at λ = 530 nm. **f**, Measured signals from the intensity and phase ports of a micro-disc resonator with a 15-μm radius at λ = 530 nm, showing one strongly over-coupled and two under-coupled whispering gallery modes. The FSR of this micro-disc resonator is ~53 mW in units of heater power.

IX. Calculation of Q-factor and finesse of the devices

The loaded Q-factor of a device is calculated by $Q_L = \lambda/\Delta\lambda$, where λ is the source wavelength, and $\Delta\lambda$ is the linewidth of the resonance dip of the transmission from the intensity port of the device. The intensity port transmission is initially measured as a function of heater power and should be converted into a curve as a function of wavelength to extract $\Delta\lambda$. For devices tested at the green wavelength, the conversion coefficient between heater power and wavelength is measured by tuning the wavelength of the source and simultaneously monitoring the heater power at the center of the resonance. For devices tested at the blue wavelength, the conversion coefficient is estimated by dividing the measured free spectral range (FSR) of the device in units of heater power by the FSR in units of wavelength determined from finite-difference time-domain (FDTD) simulations.

The intrinsic Q-factor of a device is calculated by $Q_o = Q_L(1 + \gamma_e/\gamma_o)$, where Q_L is the loaded Q-factor calculated as above, and γ_e/γ_o is calculated from T_0 using (S7).

The finesse factor of a device is calculated by $F = \mathrm{FSR}/\Delta\lambda$, where $\Delta\lambda$ is determined as above. For devices tested at the blue wavelength, the FSR is estimated from FDTD simulations, while for devices tested at the green wavelength, the FSR is determined from measurements.

The propagation loss of a device in dB per unit distance is calculated by $\alpha = 10\log_{10} e \cdot \lambda/(Q_o \cdot \mathrm{FSR} \cdot R)$ [C. Xiong *et al*., *New J. Phys.* **14**, 095014 (2012); P. Rabiei *et al*., *J. Lightwave Technol*. **20**, 1968 (2002)], where R is the radius of the device. For the adiabatic micro-ring device with R=10 μm and operating at λ=530 nm (**Figs. 3a** and **3b**), the linewidth in units of heating power is 1.3 mW and the conversion coefficient is 25 mW/nm, from which the loaded and intrinsic Q-factors are calculated to be 1.0×10^4 and 2.1×10^5, respectively; the FSR is 2.4 nm, from which the finesse factor is calculated to be 46, and the propagation loss is calculated to be 4.6 dB/cm.

For the micro-disc device with R=15 μm and operating at λ=530 nm (**Fig. S9**), the linewidth in units of heating power is 0.74 mW and the conversion coefficient is 31 mW/nm, from which the loaded and intrinsic Q-factors are calculated to be 2.2×10^4 and 3.6×10^5, respectively; the FSR is 1.7 nm, from which the finesse factor is calculated to be 71, and the propagation loss is calculated to be 2.6 dB/cm.

For the adiabatic micro-ring device with R=10 μm and operating at λ=488 nm (**Figs. 3c** and **3d**), the linewidth in units of heating power is 2.1 mW and the conversion coefficient is 15 mW/nm, from which the loaded and intrinsic Q-factors are calculated to be 3.5×10^3 and 1.1×10^5, respectively; the FSR is 2.0 nm, from which the finesse factor is calculated to be 14, and the propagation loss is calculated to be 9.6 dB/cm.

The effective propagation distance of a whispering gallery mode in a micro-ring can be estimated as the product between its circumference and the finesse factor. Take our SiN adiabatic micro-ring operating at λ=530 nm (**Figs. 3a** and **3b**) as an example, it has a radius of 10 μm and a finesse factor of 46. Thus, the effective propagation distance of light within the device is ~2,890 μm=2.89 mm. This device has a modulation loss of 0.87 dB (**Fig. 3a**). Note that this device supports a single whispering gallery mode because the narrow section of the adiabatic micro-ring is only 300 nm wide (wide section is 1.7 μm in width).

From a literature search on the attenuation coefficient of SiN waveguides in the visible, we found that the attenuation coefficient is generally lower for longer wavelengths and wider waveguides, and that for 300-nm wide single-mode SiN waveguides at λ=~530 nm the attenuation coefficient is 1.5–8.2 dB/cm. For example, see two papers cited in the main text: Refs. [26,27]. Therefore, a straight waveguide with a length equal to the effective propagation distance of light within our green adiabatic micro-ring of 2.89 mm would have an optical loss of 1.5–8.2 dB/cm × 2.89 mm =0.43–2.37 dB. The modulation loss of 0.87 dB of our single-mode adiabatic micro-ring at λ=530 nm is near the lower end of this range. Our adiabatic micro-ring operating at the blue wavelength of λ=488 nm (**Figs. 3c** and **3d**) has a modulation loss of only 0.61 dB.

Although adiabatically widened waveguides are infrequently used compared to waveguides with uniform width, we believe that using adiabaticity will certainly reduce evanescent fields at the waveguide sidewalls and associated sidewall scattering losses, which will result in smaller propagation losses as we observed in adiabatic micro-rings.

X. Conventional thermo-optical phase shifters based on waveguides

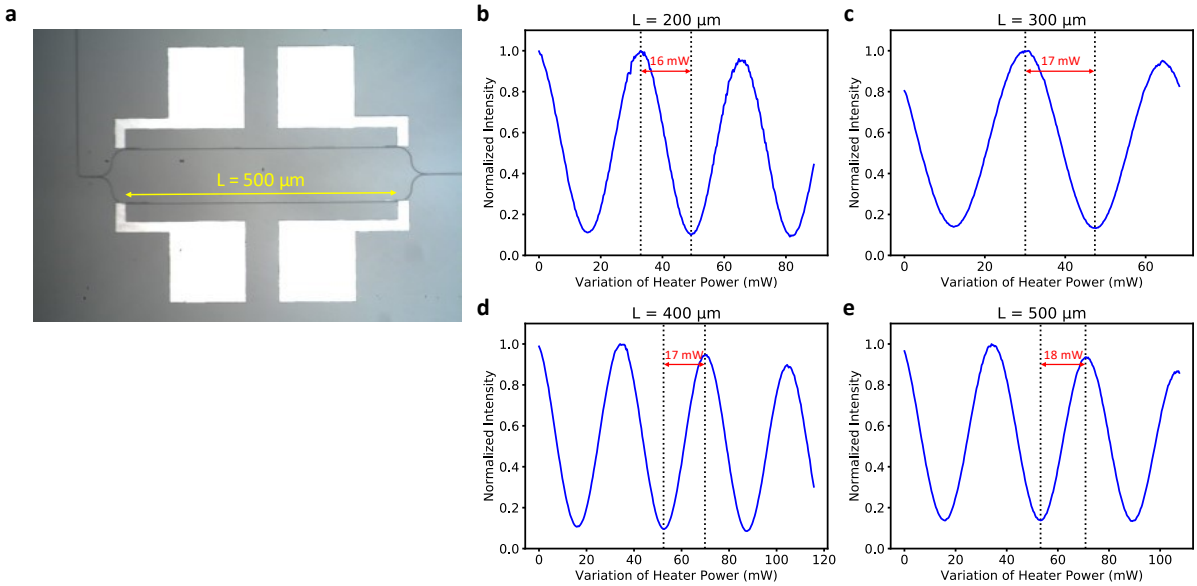

Fig. S10 | a, Microscope image of a SiN Mach-Zehnder interferometer (MZI). The length of the MZI arms is L=500 μm. Micro-heaters of the same designs (i.e., Pt wire thickness, separation between micro-heaters and SiN waveguides) as those in the devices based on micro-resonators are used. **b-e,** Measured interference signals of four MZIs at λ=488 nm as a function of heating power applied to one of the arms, showing that a heating power of ~17 mW is needed to achieve π phase modulation. The length of the MZI arms ranges from 200 to 500 μm.

XI. Modulation speed measurements and simulations

Figure S11 shows measured output signals of three adiabatic micro-ring devices and three waveguide-based phase modulators at λ = 488 nm, driven by square-waves of heater power. Time constants of the rising and falling edges of the signals are extracted by fitting the 10%-90% portion of the edges by an exponential function with a single time constant. Note that in micro-resonators the relation between the heater power and the phase response is not strictly linear (see, for example, **Fig. S3**); therefore, the rising and falling edges of the temporal traces can only be fit with an exponential function when a device operates near the center of its resonance where the heater power-phase relation is approximately linear. Once the heater power exceeds the central portion of the optical resonance, the modulated signal becomes deformed (e.g., rising edge in **b** and falling edge in **c**), and no attempt is made to extract time constant in these cases.

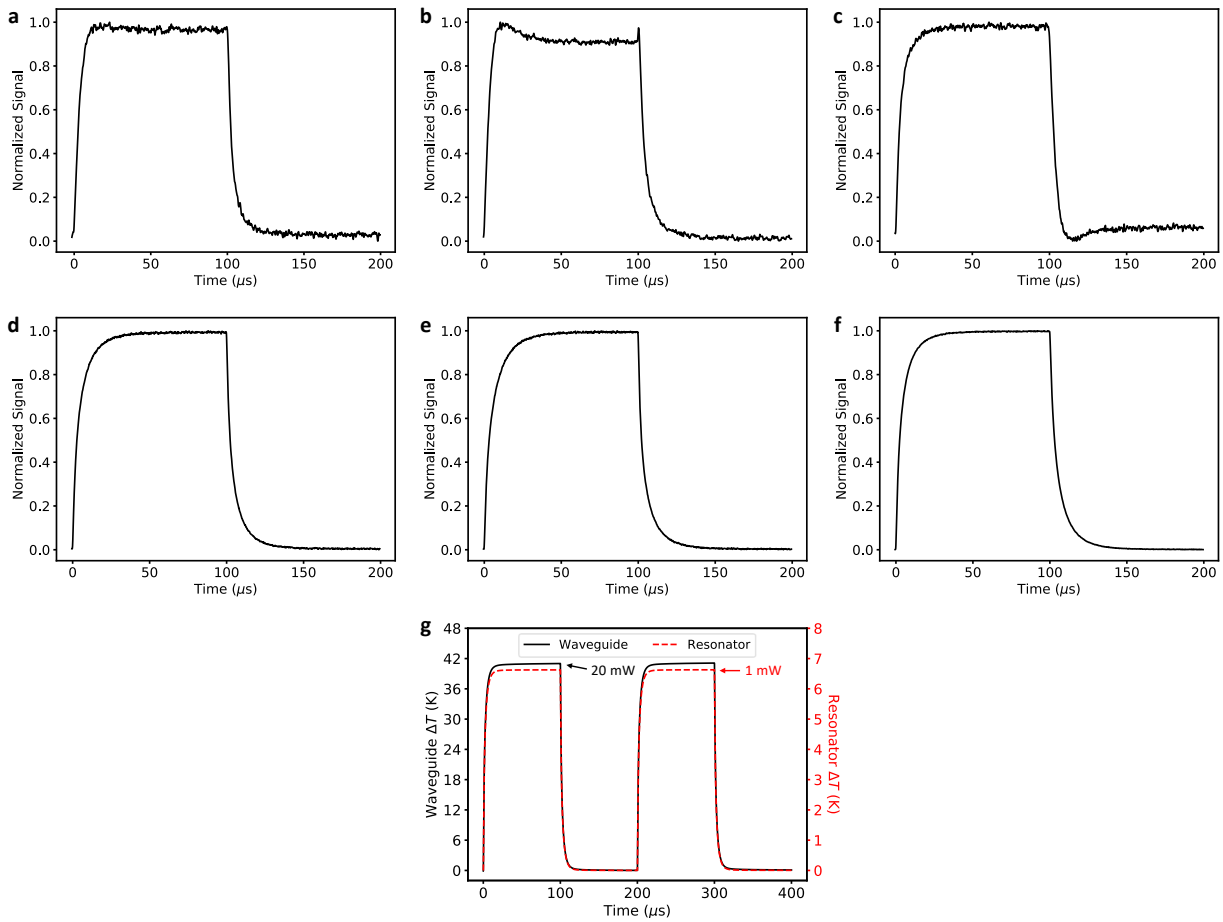

Fig. S11 | a-c, Measured signals at the phase ports of three adiabatic micro-ring devices at λ = 488 nm, driven by square-waves of heater power of a repetition rate of 5 kHz. Low-pass filtering of 500 kHz is applied to the signals to reduce noise. **d-f,** Measured signals of three waveguide-based phase modulators at λ = 488 nm, driven by square-waves of heater power of a repetition rate of 5 kHz. The lengths of the waveguides are 200 μm, 300 μm and 400 μm, respectively. Low-pass filtering of 1 MHz is applied to the signals to reduce noise. **g,** Simulated temperature evolutions in a micro-ring resonator (20 μm in diameter) and in a waveguide-based phase modulator (200 μm in length), caused by square-waves of heating power (peak power of 1 mW for the micro-ring and of 20 mW for the waveguide-based phase modulator).

XII. Whispering-gallery modes of micro-ring resonators

Figure S12 shows finite-element method (FEM) simulations of the fundamental TE and TM whispering-gallery modes of micro-ring resonators with a fixed outer radius R of 10 μm and varying width w. As w increases from 0.3 μm to 1.7 μm, the mode shifts towards the center of the micro-ring, reducing the overlap with the outer sidewall (**Fig. S12b** and **c**). The center of mode is quantified as $\langle x \rangle = \iint x|E|^2 dA \,/\, \iint |E|^2 dA$. The mode overlap with the outer sidewall is quantified as $\text{Sidewall Intensity} = \iint_{-\delta<x<\delta} |E|^2 dA \,/\, \iint |E|^2 dA$, where $\delta = 30$ nm is chosen. $\langle x \rangle$ and Sidewall Intensity as functions of w are shown in **Fig. S12d** and **e**, respectively. Both quantities decrease as w increases from 0.3 μm to ~0.7 μm, and stabilize when w further increases. In the case of a micro-disc where w=R, the quantities will be the same as the

stabilized values. The results show that Sidewall Intensity at $w > 1.0$ μm is approximately 1/4 of its value at w=0.3 μm, indicating that the whispering-gallery mode at the wide section of an adiabatic micro-ring will experience significantly less sidewall scattering than at the narrow section. **Figure S12f** and **g** show variation of the effective modal index, δn_{eff}, of the fundamental TE and TM modes, respectively, when the height of micro-ring, h, or the width of the micro-ring, w, varies by 10 nm. The variation of n_{eff} is significantly larger when δh=10 nm, compared to the case when δw=10 nm, indicating that the resonant wavelength of the micro-ring is more sensitive to the variation of height than to the variation of width. When δw=10 nm, δn_{eff} decreases significantly as w increases from 0.3 μm to ~0.5 μm, and stabilizes when w further increases, indicating that the variation of resonant wavelength caused by δw can be reduced by increasing the ring width or by using the adiabatic micro-ring.

The gradient of heating power required to align the device resonance to the laser frequency is measured to be 1.60 mW/mm for the adiabatic micro-rings and 5.44 mW/mm for the regular micro-rings (**Fig. 4b** of the main text). The heating power needed to shift the resonance across one FSR is measured to be 30 mW for the adiabatic micro-rings and 33 mW for the regular micro-rings. Using the conversion coefficient between heating power and wavelength from Supplementary Section IX, the gradient of resonant wavelength, $|\nabla\lambda_{\text{res}}|$, is then calculated to be 0.107 nm/mm for the adiabatic micro-rings and 0.363 nm/mm for the regular micro-rings. The FSR of the two types of devices is 2.0 nm and 2.2 nm, respectively. The gradient of the effective modal index, $|\nabla n_{\text{eff}}|$, can be evaluated by using $|\nabla n_{\text{eff}}| = \delta n_{\text{FSR}}|\nabla\lambda_{\text{res}}|/\text{FSR}$, where $\delta n_{\text{FSR}} = \lambda/2\pi R = 7.77 \times 10^{-3}$ is the change of effective modal index needed to shift the resonant wavelength by one FSR. $|\nabla n_{\text{eff}}|$ is thus calculated to be 4.16×10^{-4} /mm for the adiabatic micro-rings and 1.28×10^{-3} /mm for the regular micro-rings. Using $|\nabla n_{\text{eff}}| = \delta n_{\text{eff}}/\delta w \cdot |\nabla w| + \delta n_{\text{eff}}/\delta h \cdot |\nabla h|$, the variation gradients of w and h, $|\nabla w|$ and $|\nabla h|$, can then be solved based on $\delta n_{\text{eff}}/\delta w$ and $\delta n_{\text{eff}}/\delta h$ from simulations. Results in **Fig. S12g** show that for the fundamental TM modes, $\delta n_{\text{eff}}/\delta w$=$3.65\times10^{-4}$ /nm for the regular micro-rings (w=0.3 μm) and $\delta n_{\text{eff}}/\delta w$=$4.3\times10^{-5}$ /nm for the adiabatic micro-rings (w averaged from 0.3 to 1.7 μm), whereas $\delta n_{\text{eff}}/\delta h$=$1.75\times10^{-3}$ /nm for both types of devices. The variation gradients of w and h on the fabricated chip are thus estimated to be $|\nabla w|$=2.7 nm/mm and $|\nabla h|$=0.17 nm/mm, respectively.

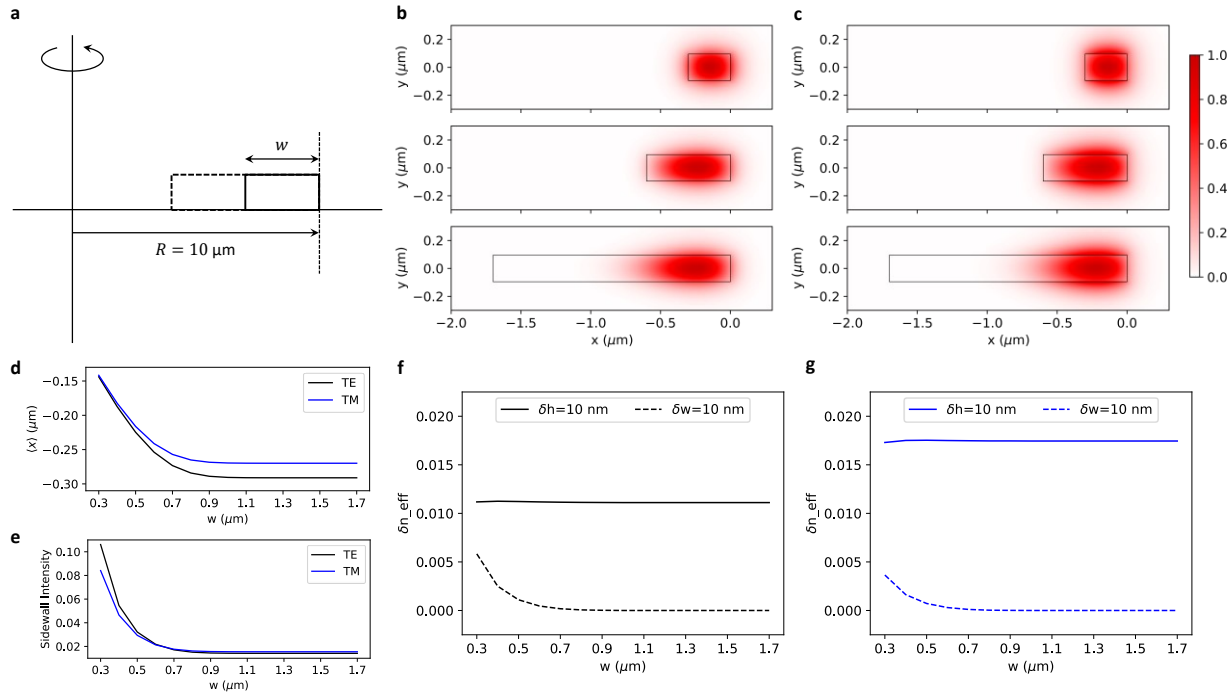

Fig. S12 | a, Schematic of the cross-section of a micro-ring resonator with an outer radius $R = 10$ μm, 190-nm height and varying width w. **b** and **c**, Simulated $|E|$ of the fundamental TE and TM whispering-gallery modes of three micro-rings with different waveguide width. From top to bottom: $w = 0.3$, 0.6 and 1.7 μm. **d** and **e**, Simulated $\langle x \rangle$ and Sidewall Intensity as a function of w. **f** and **g**, Simulated δn_{eff} of the fundamental TE and TM whispering-gallery modes of micro-rings with varying dimensions as a function of w.

XIII. Robustness of adiabatic micro-rings against fabrication variations

In this section, we compare the fabrication tolerance of adiabatic micro-rings with that of regular micro-rings (with a constant waveguide width) and that of waveguide phase shifters. We will demonstrate that among the three types of devices the adiabatic micro-ring has the highest robustness against fabrication variations, because the delocalization of modes at its wide section makes the modal refractive index insensitive to the variation of the waveguide dimensions.

<u>Comparison between adiabatic and regular micro-rings:</u> FDTD simulations show that intensity transmission at the center of resonance, T_0, decreases when RMS sidewall roughness increases (**Fig. S13a**). For example, when the RMS roughness increases to 30 nm, T_0 of the regular micro-ring decreases drastically to 0.57, while T_0 of the adiabatic micro-ring decreases to 0.89. Simulations also show that the shift of resonant wavelength caused by the variation of ring width of the regular micro-ring is about three times higher than that of the adiabatic micro-ring (**Fig. S13b**).

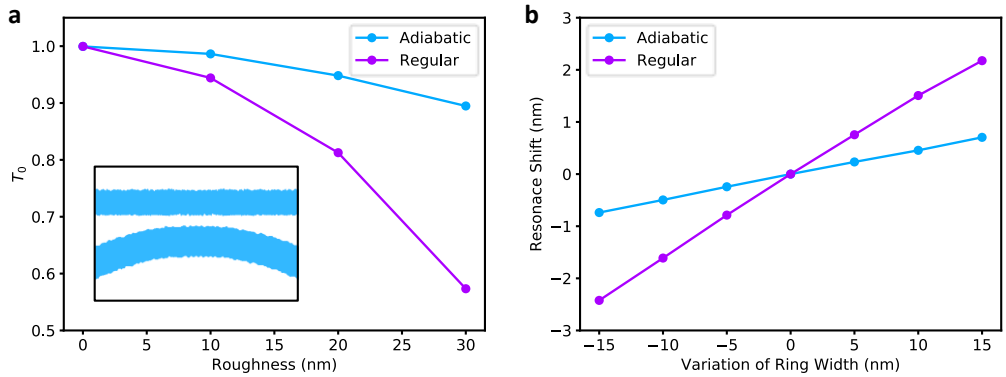

Fig. S13 | a, Simulated intensity transmission, T_0, at the center of resonance as a function of sidewall roughness at λ = 530 nm. The two types of resonators have the same diameter except that the regular micro-rings have a constant waveguide width equal to that of the narrowest section of the adiabatic micro-rings. Inset: Schematic of sidewall roughness used in simulations. The correlation length of the sidewall roughness is assumed to be 10 nm. **b,** Simulated resonance shift as a function of ring width variation at λ = 530 nm.

<u>Comparison between adiabatic micro-rings and waveguide phase shifters:</u> Assume fabrication variations introduce a change δn_{ring} in the effective modal index $n_{\text{ring}}$of an adiabatic micro-ring, the corresponding change in resonant wavelength $\delta\lambda_{\text{res}}$ is

$$\frac{\delta\lambda_{\text{res}}}{\lambda_{\text{res}}} = \frac{\delta n_{\text{ring}}}{n_{\text{ring}}}. \text{ (S26)}$$

The change in phase response of the adiabatic micro-wing, $\delta\phi_{\text{ring}}$, is

$$\frac{\delta\phi_{\text{ring}}}{\pi} = \frac{\delta\lambda_{\text{res}}}{\Delta\lambda}, \text{ (S27)}$$

considering that the linewidth of the resonance, $\Delta\lambda$, is associated with an approximately π phase shift (Supplementary Information I).

The linewidth of the resonance is further related to the loaded Q-factor Q_L via

$$Q_L = \frac{\lambda_{\text{res}}}{\Delta\lambda}. \text{ (S28)}$$

From the above relations (S26)-(S28) we can derive the change in phase response of the adiabatic micro-ring as

$$\delta\phi_{\text{ring}} = \pi Q_L \frac{\delta n_{\text{ring}}}{n_{\text{ring}}}. \text{ (S29)}$$

The change in phase response of a waveguide-based phase shifter is

$$\delta\phi_{\text{wg}} = \delta n_{\text{wg}} \frac{2\pi}{\lambda} L, \text{ (S30)}$$

where δn_{wg} is the change in modal index of the waveguide caused by fabrication variations, and L is the length of the waveguide.

Our full-wave simulations show that $\delta n_{\text{ring}}/\delta w$ =4.3×10^{-5} /nm and $\delta n_{\text{ring}}/\delta h$ =1.75×10^{-3} /nm for an adiabatic micro-ring resonator with a 10-μm outer radius operating at λ=488 nm with a quasi-TM guided mode, while $\delta n_{\text{wg}}/\delta w$=5.85×10^{-4} /nm and $\delta n_{\text{wg}}/\delta h$=1.6×10^{-3} /nm for a waveguide phase shifter with a waveguide width of 250 nm and a quasi-TM guided mode, where δw and δh are, respectively, fabrication-induced variations of the waveguide width and height. From the fabricated micro-ring devices, we have extracted the variation gradients of w and h to be $|\nabla w|$ =2.7 nm/mm and $|\nabla h|$ =0.17 nm/mm (Supplementary Section XII). The variation gradients of n_{ring} and n_{wg} are thus estimated to be

$$|\nabla n_{\text{ring}}| = \delta n_{\text{ring}}/\delta w \times |\nabla w| + \delta n_{\text{ring}}/\delta h \times |\nabla h| = 4.1\times10^{-4}\ /\text{mm} \quad \text{(S31)}$$

and

$$|\nabla n_{\text{wg}}| = \delta n_{\text{wg}}/\delta w \times |\nabla w| + \delta n_{\text{wg}}/\delta h \times |\nabla h| = 1.9\times10^{-3}\ /\text{mm}. \quad \text{(S32)}$$

$|\nabla n_{\text{ring}}|$ is approximately 5 times smaller than $|\nabla n_{\text{wg}}|$ primarily because the model index of the widened section of the adiabatic micro-ring is robust against fabrication-induced variations of the waveguide width (i.e., $\delta n_{\text{ring}}/\delta w$ is one order of magnitude smaller than $\delta n_{\text{wg}}/\delta w$). As $|\nabla n_{\text{wg}}|$ is a few times larger than $|\nabla n_{\text{ring}}|$, the phase error of the waveguide-based phase shifters and the thermal bias needed to correct the error in n_{wg} should be a few times larger than that of the adiabatic micro-rings.

Using a set of parameters observed or used in our fabricated devices (i.e., loaded Q-factor of the adiabatic micro-ring of Q_L=3.5×10^3, effective modal index of n_{ring}=2.0, length of the waveguide phase shifter of L=400 μm), the variation gradient of phase response is estimated according to (S29)-(S32) to be

$$|\nabla \phi_{\text{ring}}| = \pi Q_L \frac{|\nabla n_{\text{ring}}|}{n_{\text{ring}}} = 2.3 \text{ radians/mm} \quad \text{(S33)}$$

for the adiabatic micro-ring and

$$|\nabla \phi_{\text{wg}}| = |\nabla n_{\text{wg}}| \frac{2\pi}{\lambda} L = 9.8 \text{ radians/mm} \quad \text{(S34)}$$

for the waveguide-based phase shifter; that is, the phase error caused by systematic variations in waveguide width and height of adiabatic micro-rings is a few times smaller than that of waveguide-based phase shifters. This is not surprising: the phase response of a waveguide should exhibit a fabrication sensitivity similar to that of a regular micro-ring (a regular micro-ring is effectively a waveguide connected head to tail), and an adiabatic micro-ring should exhibit improved robustness against fabrication variations compared to both straight waveguides and conventional micro-rings.

XIV. Capability of forming compact arrays of phase modulators

To achieve on-chip, large-scale integration of phase modulators, the footprint of individual devices must be minimized and the power consumption of the whole chip needs to be in check; in the case of thermo-optical modulators, the thermal crosstalk between adjacent devices has to be minimized to reduce the amount of phase error. Our FDTD simulations show that the outer radius of the adiabatic micro-ring resonator can be reduced to 4-5 μm without causing a significant bending loss (**Figs. S14**, **S15** and **S16**).

Figure S14c shows simulated spatial distributions of excess temperatures (i.e., local temperature minus heat sink temperature) normalized to the peak temperature in the device plane for a waveguide-based phase

shifter and a micro-ring resonator with a 4-μm outer radius. The simulations are conducted using COMSOL Multiphysics and show the following relation between the perturbation to the effective modal index δn, which is proportional to the normalized excess temperature, and the device separation:

Table S1

δn due to thermal crosstalk	Waveguide separation w_{wg} (μm)	Micro-ring separation w_{ring} (μm)
10%	4.4	7.5
5%	6.0	8.7
2%	9.4	10.5
1%	23.8	12.3

The footprint of the waveguide phase shifter can then be estimated as $S_{wg} = L_{wg} \times w_{wg}$, where L_{wg} is the waveguide length (taken to be 400 μm, but is typically much longer in devices reported in the literature), and that of the micro-ring as $S_{ring} = w_{ring}^2$:

Table S2

δn	S_{wg} (μm^2)	S_{ring} (μm^2)	S_{wg} / S_{ring}
10%	1760	56.25	31.3
5%	2400	75.69	31.7
2%	3760	110.25	34.1
1%	9520	151.29	62.9

Thus, we can see from the last column of the above table that if the phase error introduced by thermal crosstalk is to be kept within 10%, using micro-rings can reduce the device footprint by more than one order of magnitude compared to using waveguide-based phase shifters.

The resonator-based phase modulators have the potential to greatly reduce the power budget of the integrated photonic chip. Assuming that the double-resonator design described in **Fig. S3b** is used as the pixel of the phased array, a 2π phase modulation can be achieved using a heating power of 0.85×2=1.70 mW per pixel (according to measured power consumption for π phase modulation in **Fig. 3b** of the main text); therefore, the power consumption for thermo-optically modulating a 1,024-element array is ~1.74 W. Considering the measured heating-power gradient, 1.60 mW/mm, across the chip needed to align the resonant frequencies of the adiabatic micro-rings to the laser frequency (**Fig. 4b** of the main text), and assuming S_{ring}=151.29 μm^2 for each resonator, the 1,024-element array would require an extra bias power of ~0.91 W, and thus the total power consumption for the 2D array is estimated to be 1.74+0.91=2.65 W. In comparison, a 1,024-element array of waveguide phase shifters would consume a total power of 40.96 W for thermo-optical modulation (according to measured power consumption for π phase modulation in **Fig. 3e** of the main text).

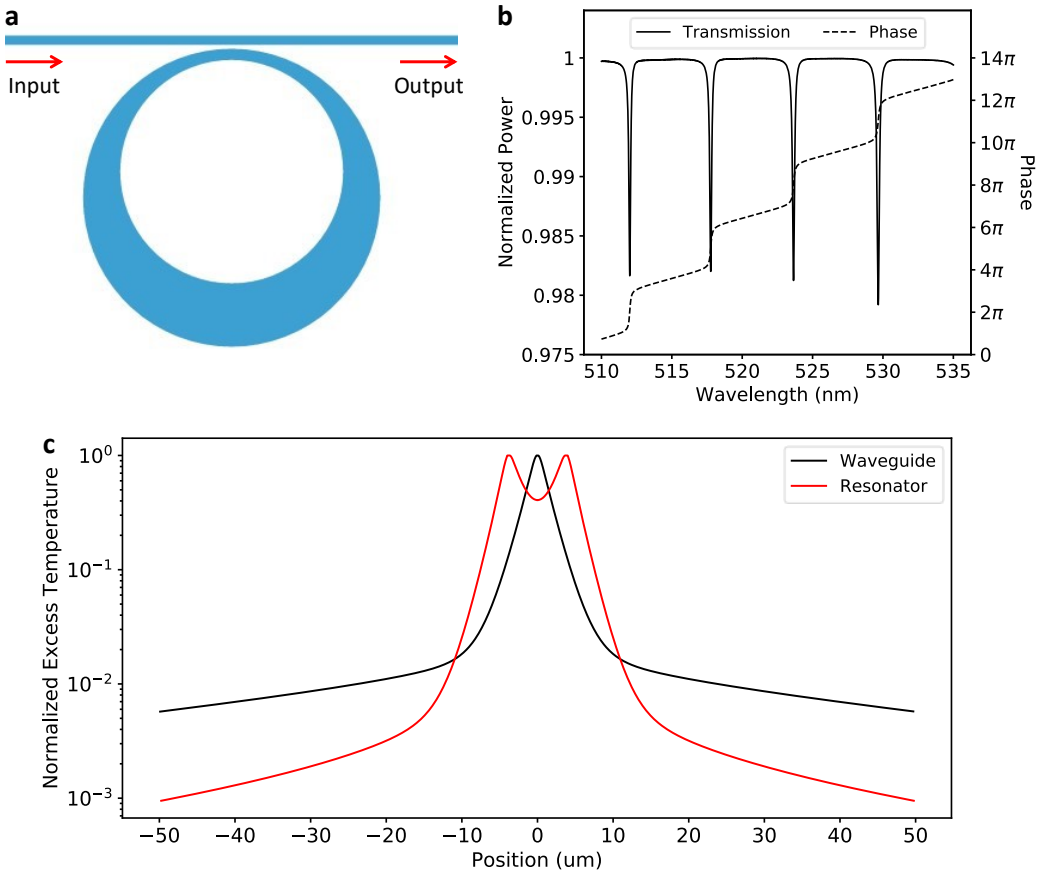

Fig. S14 | a, Schematic of an adiabatic micro-ring resonator with a 4-μm outer radius. **b,** Simulated spectra of power transmission and phase response of the device shown in **a** at the green wavelengths. The resonator operates in the strongly over-coupled regime, with negligible bending losses and a 2π phase change across each resonance. No scattering and absorption losses are included in the simulations; therefore, the dips in the transmission spectrum are solely caused by bending losses. **c,** Simulated spatial distributions of temperature around a thermo-optically tuned waveguide phase modulator and a micro-ring resonator with a 4-μm outer radius. Plotted are excess temperatures (i.e., local temperature minus ambient or heat sink temperature) normalized to the peak temperature along a straight line at the middle level of the SiN layer: in the case of the waveguide phase shifter, the line is normal to the waveguide; in the case of the micro-ring resonator, the line is through the center of the micro-ring. The temperature gradient is larger near a micro-ring compared to a waveguide is due to the fact that the micro-heater is localized in the micro-ring device (becoming a point heater when the micro-ring radius shrinks to zero) but is extensive (effectively a linear source of heat) in the waveguide device.

XV. Adiabatic micro-ring phase shifter operating over the entire visible range

In this section we will demonstrate using full-wave simulations that suitably designed adiabatic micro-rings can operate in the strongly over-coupled regime over the entire visible spectrum, and thus can be used as phase shifters with minimal modulation losses for light of any color in the visible. Two sets of simulations and their results will be shown, one based on modal indices and propagation losses extracted from our experimental adiabatic micro-rings operating at the blue and green spectra, and the other based on modal

indices and propagation losses extracted from foundry-fabricated SiN waveguides over the entire visible spectral range (Ref. [27] in the main text).

(1) Adiabatic micro-ring design and simulation using complex refractive indices extracted from our SiN micro-rings. The adiabatic micro-ring (same as the one in **Fig. S14a**) is defined by an outer circle with a radius of 4 μm and an inner circle with a radius of 3 μm, and the distance between the centers of the two circles is 700 nm; therefore, the narrowest section of the adiabatic micro-ring is 300 nm in width and the widest section1.7 μm in width. The adiabatic micro-ring is coupled to a straight waveguide with a width of 250 nm, and the resonator-waveguide gap size is 70 nm.

Scattering loss at sidewall roughness is a major source of optical losses in our fabricated devices, dominating over other loss mechanisms, including scattering of the coupler, material absorption, and bending loss in the resonator (Supplementary Section III). To include the effect of sidewall scattering loss in our FDTD simulations, we assign an effective extinction coefficient to the complex refractive index of SiN (instead of building a physical model of micro-rings with roughened sidewalls, because the RMS and correlation length of the roughness in our fabricated devices are not quantified). This is done following three steps:

(a) The attenuation coefficient of our fabricated devices operating at λ_1=530 nm and λ_2=488 nm (**Fig. 3a-d**) is calculated to be α_1=1.1 cm^{-1} and α_2=2.2 cm^{-1}, respectively, using $\alpha = \lambda_0/(Q \cdot R \cdot \mathrm{FSR})$ [X. Ji, F. A. S. Barbosa, A. Bryant, J. Cardenas, S. P. Roberts and M. Lipson, "High quality factor Si3N4 ring resonators achieved by surface roughness reduction," paper SM2R.3 in 2016 Conference on Lasers and Electro-Optics (CLEO), San Jose, CA, 2016]. Here, Q is the intrinsic quality factor, R is the outer radius of the micro-ring, and FSR is the free spectral range.

(b) The effective imaginary part of the complex refractive index of the SiN micro-ring is then calculated to be κ_1=4.6×10^{-6} and κ_2=8.5×10^{-6}, respectively, using $\kappa = \alpha\lambda_0/4\pi$. Note that the difference in the two values originates primarily from the difference in fabrication quality of the green and blue devices, rather than wavelengths.

(c) We choose the larger κ of 8.5×10^{-6} among the above two values and keep it a constant in our FDTD simulations. Physically, Rayleigh scattering by surface roughness is stronger at shorter wavelengths, but whispering-gallery modes at shorter wavelengths are more confined within SiN with less evanescent fields at the sidewalls. The balance between these two effects could lead to a relatively constant scattering loss (and an effective κ) as a function of wavelength.

In this way, our FDTD simulations take into consideration a combined effect of scattering loss due to the waveguide-resonator coupling, scattering loss caused by sidewall roughness (modeled by an equivalent material absorption), and bending loss. **Figure S15 a** and **b** show simulated transmission spectra of the adiabatic micro-ring resonator for quasi-TE and quasi-TM waveguide modes, respectively, over the λ=450-700 nm wavelength range. The results show that the device has a modulation loss ranging from 0.3 to 0.7 dB (**Fig. S15 a**, **b**), corresponding to γ_e/γ_o ranging from 25 to 65 (**Fig. S15 c**, **d**). That is, the device operates in the strongly over-coupled regime for all resonances within the simulated spectral range. **Figure S15 c** and **d** further show the Finesse factor for all resonances. The Finesse factor ranges from ~40 in the blue to ~6 in the red for quasi-TE waveguide mode, and from ~64 in the blue to ~10 in the red for quasi-TM waveguide mode; this corresponds to a reduction in the power consumption of thermo-optical modulation (compared to waveguide-based phase shifters) by a factor of ~3 to ~32, depending on wavelength and polarization of the guided mode. An increase of waveguide-resonator coupling at longer wavelengths (due to more extended evanescent waves) leads to increased linewidth of the resonance, and subsequently leads

to decreased Finesse factors. **Figure S15 e** and **f** show that a ~2π phase change is associated with each resonance.

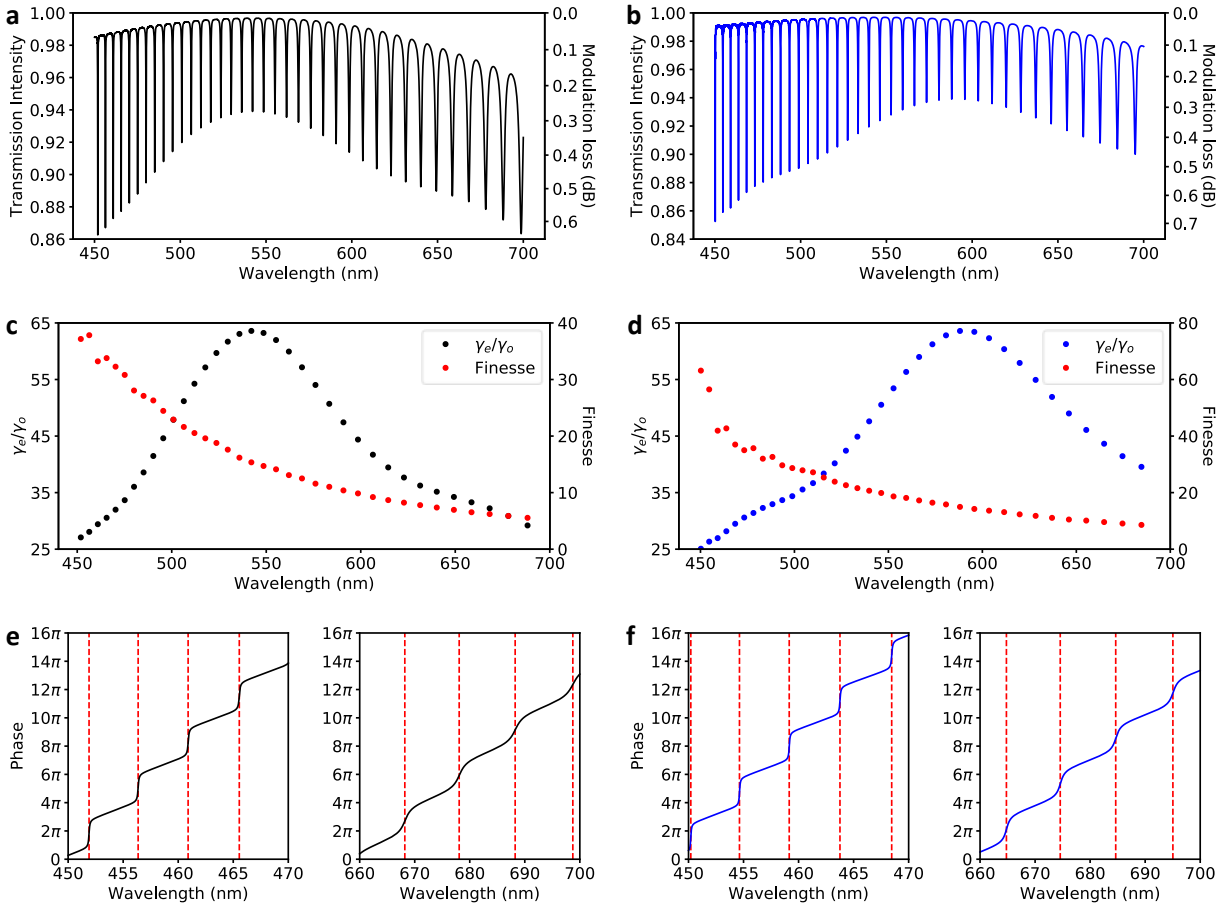

Fig. S15 | a,b Simulated transmission spectra and corresponding modulation loss of an adiabatic micro-ring resonator for quasi-TE (**a**) and quasi-TM (**b**) waveguide modes in the visible wavelength range of λ=450-700 nm. **c**,**d,** Calculated γ_e/γ_o (coupling rate / decay rate) and Finesse of the resonant modes in **a** and **b**, respectively. **e**,**f** Simulated phase responses in the blue and red wavelength ranges of the adiabatic micro-ring with quasi-TE (**e**) and quasi-TM (**f**) waveguide modes. Red dashed lines indicate the centers of the resonances. The adiabatic micro-ring resonator has a 4-μm outer radius (same as the one in **Fig. S14a**) while the gap size between the micro-ring and the straight bus waveguide is 70 nm. An imaginary refractive index of $\kappa=8.5\times10^{-6}$ is added to the SiN material in the simulations to model the scattering loss caused by sidewall roughness.

(2) Adiabatic micro-ring design and simulation using complex refractive indices extracted from Ref. [27]. We also demonstrate in simulations strongly over-coupled adiabatic micro-rings using effective complex refractive indices of SiN derived from Ref. [27] (Sacher, *et al*. *Optics Express* **27**, 37400-37418 (2019)). Reference [27] reported SiN refractive indices and propagation losses at several visible spectral bands of SiN waveguides with various widths fabricated using the Advanced Micro Foundry (AMF) processes. We use their propagation loss data of single-mode SiN waveguides (i.e., waveguide width of 250 nm and thickness of 200 nm, quasi-TE modal polarization) and conduct simulations in the wavelength

ranges of λ=430-464 nm, 466-500 nm, 502-550 nm, 552-600 nm and 602-648 nm separately. In each wavelength range, the attenuation coefficient, α, is calculated from the reported propagation loss data, and the effective imaginary part of the complex refractive index, κ, is calculated at the central wavelength. The propagation loss, α, and κ used in the simulations for the five wavelength ranges are summarized in the table below. The adiabatic micro-ring is defined by an outer circle with a radius of 5 μm and an inner circle with a radius of 4 μm, and the distance between the centers of the two circles is 700 nm. The adiabatic micro-ring is coupled to a straight waveguide with a width of 250 nm, and the resonator-waveguide gap size is 70 nm.

Table S3

Wavelength range	430-464 nm	466-500 nm	502-550 nm	552-600 nm	602-648 nm
Central wavelength	447 nm	483 nm	526 nm	576 nm	625 nm
Propagation loss (dB/cm)	10.6	8.3	5.5	4.3	3.3
Attenuation coefficient α (cm^{-1})	2.44	1.91	1.27	0.99	0.76
Imaginary part of refractive index κ	8.68×10^{-6}	7.34×10^{-6}	5.32×10^{-6}	4.54×10^{-6}	3.78×10^{-6}

Figure S16a shows simulated transmission spectra of the adiabatic micro-ring operating in quasi-TE waveguide mode in the five wavelength ranges. The results show that the device has a modulation loss ranging from 0.1 to 0.9 dB and that the loss is below 0.3 dB over the entire green and red spectra (λ=500-650 nm) (**Fig. S16a**). The ratio between the coupling rate and loss rate, γ_e/γ_o, at the resonances ranges from 20 to 150 (**Fig. S16b**); therefore, the device operates in the strongly over-coupled regime for all resonances within the simulated spectral range. **Figure S16b** further shows that the Finesse factor at the resonances ranges from ~40 in the blue to ~5 in the red, which corresponds to a reduction in the power consumption of thermo-optical modulation (compared to waveguide-based phase shifters) by a factor of ~20 to ~2.5. **Figure S16c** shows that a ~2π phase change is associated with each resonance.

Thus, we demonstrate in **Figs. S15** and S**16** that (a) a micron-sized adiabatic micro-ring can function as a phase shifter without introducing significant modulation losses, (b) it can provide 2π phase modulation for a set of discrete wavelengths in the visible, and (3) the device can support a substantial reduction of power consumption for thermo-optical modulation. The results in **Fig. S16** are particularly significant because the design is based on optical losses of foundry-fabricated SiN waveguides.

We note that compared to a waveguide phase shifter, an adiabatic micro-ring has a slightly reduced versatility: the former can operate at any wavelength, whereas the latter has to be thermo-optically tuned so that one of its many resonances matches with the laser wavelength. That is, the reduced versatility can be compensated for by extra power consumption: a properly designed adiabatic micro-ring with an integrated micro-heater to provide thermal biasing and thermo-optical tuning can be used as a low-loss phase shifter for any visible wavelength. The heating bias required for adjusting a micro-ring resonance can be reduced by using rings of larger radii (smaller FSR).

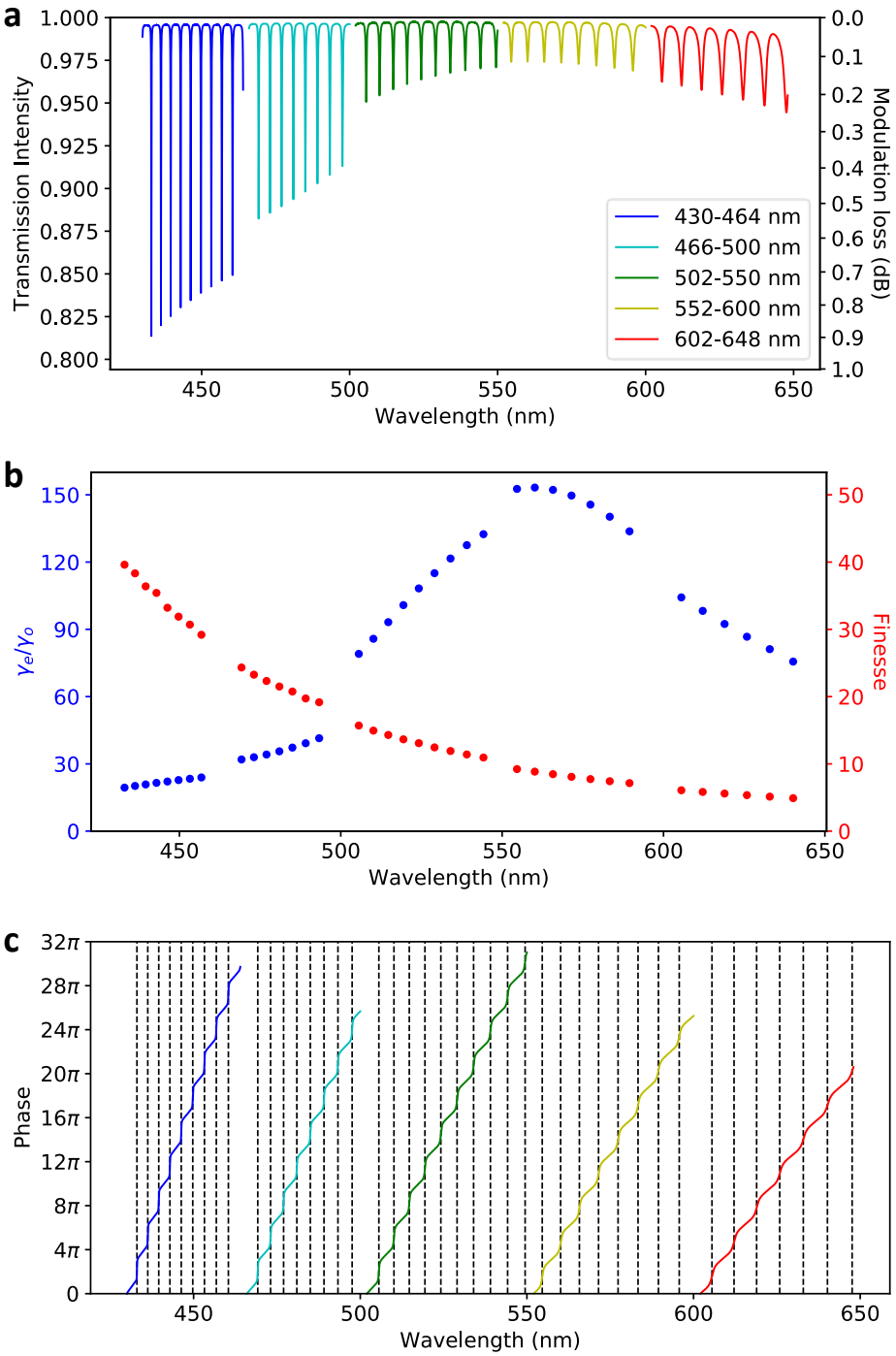

Fig. S16 | a, Simulated transmission spectrum and corresponding modulation loss of an adiabatic micro-ring resonator operating in the visible wavelength range for quasi-TE waveguide modes. The simulations are conducted using propagation losses of foundry-fabricated waveguides in Ref. [27]. **b,** Calculated γ_e/γ_o (coupling rate / decay rate) and Finesse of the resonant modes in **a**. **c**, Simulated phase response of the adiabatic micro-ring resonator. Black dashed lines indicate the centers of the resonances. The adiabatic micro-ring resonator has a 5-μm outer radius while the gap size between the micro-ring and the straight bus waveguide is 70 nm. Imaginary refractive indices of $\kappa = 8.68\times10^{-6}$, 7.34×10^{-6}, 5.32×10^{-6}, 4.54×10^{-6} and

3.78×10^{-6} are added to the SiN material in the simulations in the wavelength ranges of 430-464 nm, 466-500 nm, 502-550 nm, 552-600 nm and 602-648 nm, respectively, to model the scattering loss caused by sidewall roughness.

XVI. Strongly over-coupled micro-ring resonators at the telecom wavelengths

We have also demonstrated phase modulation with minimal modulation losses in regular SiN micro-ring resonators operating at the telecom wavelengths (λ = 1540-1610 nm). The micro-ring devices have radii of 15 to 20 μm, and the gap between the bus waveguide and the micro-ring is 150 to 200 nm. **Figure S17a** shows the geometry of two devices with a 15-μm radius, one with a straight waveguide coupler and the other a conveyor-belt coupler. **Figure S17b** shows a microscope image of a fabricated device with a 15-μm radius and a straight waveguide coupler. The SiN layer is 600-nm thick, and the Pt micro-heater is patterned on top of a 2-μm thick SiO_2 cladding layer with a radius 3 μm larger than the SiN micro-ring. The transmission spectra of the "intensity" and "phase" ports (defined in **Fig. 2b**) are measured by sweeping the source wavelength, and the power-to-wavelength conversion coefficient is determined by applying a heating power through the micro-heater and re-measuring the transmission spectra. The amplitude and phase responses as a function of wavelength are then extracted from the transmission spectra of the two output ports.

Experimental results of a device with a 15-μm radius and a straight coupler with a 150-nm waveguide-resonator gap are shown in **Figs. S17c** and **d**. The transmission drop at the center of the resonance is 0.86 dB, and a π phase change is achieved with a tuning range of 0.87 nm in wavelength, corresponding to 15 mW in heating power (power-to-wavelength conversion coefficient of 17 mW/nm). Experimental results of a second device with a 15-μm radius and a conveyor-belt coupler with a 150-nm gap are shown in **Figs. S17e** and **f**. The transmission drop at the center of the resonance is 0.61 dB, and a π phase change is achieved with a tuning range of 0.52 nm in wavelength, corresponding to 8.3 mW in heating power (power-to-wavelength conversion coefficient of 16 mW/nm). Experimental results of a third device with a 20-μm radius and a conveyor-belt coupler with a 200-nm gap are shown in **Figs. S17g** and **h**. The transmission drop at the center of the resonance is 1.27 dB, and a π phase change is achieved with a tuning range of 0.19 nm in wavelength, corresponding to 4.0 mW in heating power (power-to-wavelength conversion coefficient of 21 mW/nm). The finesse factors of the three devices are calculated to be 15, 26 and 53, respectively (using the fact that the central π phase change in the phase response curves corresponds to the linewidth of the resonance; see Supplementary Section I).

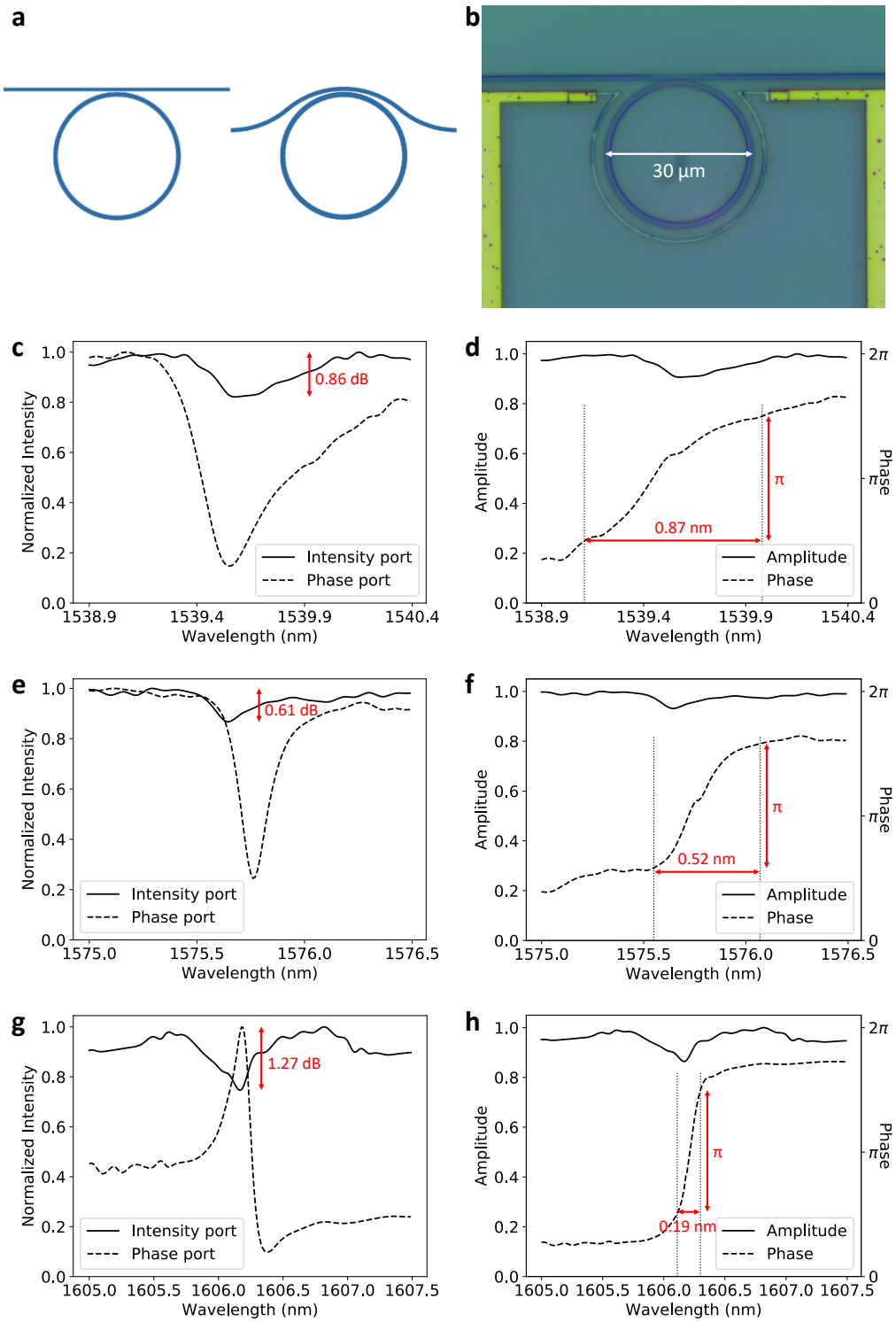

Fig. S17 | a, Geometry of regular SiN micro-ring resonators operating in the telecom spectrum, with a 15-µm radius and a straight waveguide coupler (left) or a conveyor-belt coupler (right). **b,** Microscope image of a device of a 15-µm radius. **c-h**, Measured signals from the "intensity" and "phase" ports and extracted amplitude and phase responses of a micro-ring resonator with a 15-µm radius and a straight coupler (**c** and

d), a micro-ring resonator with a 15-μm radius and a conveyor-belt coupler (**e** and **f**), and a micro-ring resonator with a 20-μm radius and a conveyor-belt coupler (**g** and **h**). The unusual phase port signal in **g** is due to an imbalance of the length of the two arms of the on-chip Mach-Zehnder interferometer.

XVII. Comparison between micro-rings and optimized waveguide phase shifters

An optimized waveguide phase modulator using the thermo-optic silicon platform in the telecom wavelength has been reported in S. Chung *et al*., Low-power thermo-optic silicon modulator for large-scale photonic integrated systems, *Optics Express* 27, 13430-13459 (2019). By folding a waveguide multiple times under a micro-heater, the phase modulator ('serpentine waveguide device') can achieve a reduction in power consumption of 9.53 times compared to a straight waveguide; it also features a compact footprint of 0.0023 mm^2 and an optical loss of 1.23 dB.

In a subsequent conference paper (S. Idres and H. Hashemi, Low-Power SiN Thermo-Optic Phase Modulator Operating in Red Visible Wavelength Range, Conference on Lasers and Electro-Optics, paper JTh2B.7 (2020)), the same research lab reported a visible serpentine phase shifter. In this work, due to the reduced modal confinement of SiN waveguides compared to Si waveguides, each SiN waveguide bend has to be sufficiently large (18 μm × 8 μm = 144 μm^2) in order to keep the bending loss sufficiently small (0.06 dB per bend). The entire device, which consists of 14 bends, occupies a footprint of 170 μm × 30 μm = 5,100 μm^2. This phase shifter can achieve a reduction in power consumption of 9.18 times compared to a straight waveguide. The device insertion loss was not reported but can be estimated by summing the bending and propagation losses of the serpentine structure.

In the following, we will compare the performance of the optimized serpentine waveguide phase shifters and strongly over-coupled resonators in both the visible and the telecom spectra. To facilitate comparison between devices, we define two figures of merit (FOMs) that take into consideration both device footprint and power consumption, the two most important device characteristics.

(1) Comparison in the visible spectrum

As reported in the main text, we have experimentally demonstrated SiN phase modulators based on adiabatic micro-ring resonators in the visible (λ=530 nm and 488 nm). The device operating at λ=530 nm can achieve P_π = 0.85 mW with only 0.87 dB optical loss (**Figs. 3a** and **b**), resulting in a reduction of power consumption of N_{reduct} = 24 compared to a control straight waveguide phase shifter (P_{π_wg} = ~20 mW). The radius of this adiabatic micro-ring is 10 μm, and thus the footprint is S_{footpr} = 314 μm^2.

The comparison of the devices in the visible (λ=~520 nm) is summarized in the following table.

Table S4

Device	SiN serpentine waveguide device in Idres *et al*. (2020)	SiN adiabatic micro-ring (10-μm radius) in **Figs. 3a** and **b**
Optical loss	1.28* dB	0.87 dB
S_{footpr}	5,100 μm^2	314 μm^2
P_π	5.35 mW	0.85 mW
N_{reduct}	9.18**	24
$FOM_1 \equiv S_{footpr}/N_{reduct}$	555.5 μm^2	13.1 μm^2

FOM$_2$ ≡ $S_{footpr} \times P_\pi$	27,285 μm^2 × mW	267 μm^2 × mW

* Theoretical best scenario (experimental insertion loss not reported in Idres *et al*. (2020)), including bending loss of 0.84 dB (0.06 dB/bend × 14 bends) and propagation loss of 0.44 dB (880 μm × 5 dB/cm, where 5 dB/cm is our experimental smallest waveguide loss).

** Idres *et al*. (2020) reported power consumption for π phase tuning P_π of 5.35 mW and that of a control straight waveguide P_{π_wg} of 49.1 mW. Thus, Nreduct = P_{π_wg}/P_π=9.18.

The comparison shows that our micro-ring devices on the basis of the FOMs is much better than the visible serpentine. Meanwhile, our device optical loss of 0.87 dB is smaller than that of the visible serpentine, which has a theoretical best scenario insertion loss of 1.28 dB.

Note that our definitions of FOM only take into consideration device power consumption and footprint, not operation bandwidth. This is because the primary applications in the visible wavelength range, such as quantum optics, optical artificial neural network, optogenetics, and AR/VR, require small footprint and low power consumption, while they do not necessarily require ultrahigh modulation speed (e.g., refresh rate of an augmented reality display just needs to be faster than the perception of the human eye; optogenetic probes just need to be much faster than the firing of a neuron, which is a few milli-seconds).

(2) Comparison in the telecom spectrum

In Supplementary Section XVI we have shown additional experimental results of phase modulation using strongly over-coupled regular SiN micro-ring resonators operating in the telecom spectrum. For example, a device with a 15-μm radius and a conveyor-belt coupler with a 150-nm waveguide-resonator gap can achieve π phase tuning with a wavelength change of 0.52 nm and a modulation loss of only 0.61 dB (**Figs. S17e** and **f**), It has a finesse factor of $F = 26$, resulting in a power reduction of $N_{reduct} = F/2 = 13$. The footprint of this device is S_{footpr} = 707 μm^2, and thus the FOM is 54 μm^2.

We also provide a theoretical estimation of the FOM of a strongly over-coupled Si micro-ring resonator using published experimental data from B. Lee *et al*., "Transmission of high-data-rate optical signals through a micrometer-scale silicon ring resonator," *Optics Letters* **31**, 2701-2703 (2006). In this paper a Si micro-ring resonator with a 10-μm radius coupled to two parallel bus waveguides is reported to have a loaded Q-factor of 20,000 and a FWHM of 0.078 nm. Assuming that the group index is $n_g = 4.3$ [W. Bogaerts *et al*., *Laser Photonics Rev.* **6**, 47–73 (2012)], the free spectral range (FSR) is calculated to be FSR $= \lambda^2/n_g L = 9.1$ nm, where L is the circumference of the micro-ring; thus, the finesse factor is $F = \frac{\text{FSR}}{\text{FWHM}} = \sim 116$. Using equation $F = \pi\sqrt{r_1 r_2 a}/(1 - r_1 r_2 a)$, the product of the two coupling coefficients r_1, r_2 and the single-pass amplitude transmission a is calculated to be $r_1 r_2 a \approx 0.973$. The resonator is operating near the critical coupling condition, i.e., $r_1 \approx r_2 a$, thus $r_2 a \approx 0.987$ and $a > 0.987$. We use $a = 0.987$ in our theoretical estimation and assume that the micro-ring is now coupled to a bus waveguide under the strongly over-coupling condition with a coupling coefficient of $r = 0.83$ (this coupling coefficient is achievable according to W. Bogaerts *et al*. (2012)), the finesse factor is then estimated to be $F = \pi\sqrt{ra}/(1 - ra) = 15.7$, corresponding to a power reduction of $N_{reduct} = F/2 = 7.86$. The transmission at the center of the resonance is estimated to be $T_0 = \frac{(r-a)^2}{(1-ra)^2} = 0.754$, corresponding to an optical modulation loss of 1.23 dB. The footprint of this device is S_{footpr} = 314 μm^2, and thus the FOM is estimated to be 40 μm^2.

The comparison of the devices in the telecom wavelength (λ=~1570 nm) is summarized in the following table.

Table S5

Device	Si serpentine waveguide device in Chung *et al*. (2019)	Experimentally demonstrated SiN micro-ring (15-μm radius)	Theoretically estimated Si micro-ring (10-μm radius)
Optical loss (dB)	1.23 dB	0.61 dB	1.23 dB
S_{footpr} (μm^2)	2,300 μm^2	707 μm^2	314 μm^2
N_{reduct}	9.53	13	7.86
FOM=S_{footpr}/N_{reduct} (μm^2)	241 μm^2	54 μm^2	40 μm^2

These results show that our experimentally demonstrated SiN micro-ring at the telecom wavelength outperforms the serpentine waveguide device in all aspects (i.e., small loss, small footprint, large reduction of power consumption), and that the theoretical Si micro-ring at the telecom wavelength can have a smaller FOM.